

# BINGO: A code for the efficient computation of the scalar bi-spectrum

**Dhiraj Kumar Hazra**

Harish-Chandra Research Institute, Chhatnag Road, Jhansi, Allahabad 211019, India<sup>‡</sup>.

**L. Sriramkumar**

Department of Physics, Indian Institute of Technology Madras, Chennai 600036, India.

E-mail: [sriram@physics.iitm.ac.in](mailto:sriram@physics.iitm.ac.in)

**Jérôme Martin**

Institut d'Astrophysique de Paris, UMR7095-CNRS, Université Pierre et Marie Curie, 98bis boulevard Arago, 75014 Paris, France.

E-mail: [jmartin@iap.fr](mailto:jmartin@iap.fr)

**Abstract.** We present a new and accurate Fortran code, the BI-spectra and Non-Gaussianity Operator (BINGO), for the efficient numerical computation of the scalar bi-spectrum and the non-Gaussianity parameter  $f_{\text{NL}}$  in single field inflationary models involving the canonical scalar field. The code can calculate all the different contributions to the bi-spectrum and the parameter  $f_{\text{NL}}$  for an arbitrary triangular configuration of the wavevectors. Focusing firstly on the equilateral limit, we illustrate the accuracy of BINGO by comparing the results from the code with the spectral dependence of the bi-spectrum expected in power law inflation. Then, considering an arbitrary triangular configuration, we contrast the numerical results with the analytical expression available in the slow roll limit, for, say, the case of the conventional quadratic potential. Considering a non-trivial scenario involving deviations from slow roll, we compare the results from the code with the analytical results that have recently been obtained in the case of the Starobinsky model in the equilateral limit. As an immediate application, we utilize BINGO to examine of the power of the non-Gaussianity parameter  $f_{\text{NL}}$  to discriminate between various inflationary models that admit departures from slow roll and lead to similar features in the scalar power spectrum. We close with a summary and discussion on the implications of the results we obtain.

PACS numbers: 98.80.Cq, 98.70.Vc

<sup>‡</sup> Current affiliation: Asia Pacific Center for Theoretical Physics, Pohang, Gyeongbuk 790-784, Korea.  
E-mail: [dhiraj@apctp.org](mailto:dhiraj@apctp.org).

## 1. Non-Gaussianities and primordial features

Over the last half-a-dozen years, it has been increasingly realized that the detection of non-Gaussianities in the primordial perturbations can considerably help in constraining the inflationary models (see Refs. [1, 2, 3]; for early efforts in this direction, see Refs. [4]). In particular, the detection of a high value for the dimensionless non-Gaussianity parameter  $f_{\text{NL}}$  that is often used to describe the amplitude of the scalar bi-spectrum can rule out a wide class of models. For instance, if the extent of non-Gaussianity actually proves to be as large as the mean values of  $f_{\text{NL}}$  arrived at from the WMAP data (see Refs. [5, 6, 7]; in this context, also see Refs. [8, 9]), then canonical scalar field models that lead to slow roll inflation and nearly scale invariant primordial spectra will cease to be consistent with the data.

However, the evaluation of the scalar bi-spectrum in a generic inflationary model proves to be a non-trivial task [10]. Often, it is the slow roll approximation that is resorted to in order to arrive at analytical expressions for the scalar bi-spectrum and the non-Gaussianity parameter  $f_{\text{NL}}$  [1, 2]. While the slow roll approximation can actually encompass a relatively wide class of models, evidently, the approach will cease to be valid when departures from slow roll occur. In such situations, one is often forced to approach the problem numerically. In this work, we shall present a new and accurate Fortran code, the BI-spectra and Non-Gaussianity Operator (BINGO), to numerically evaluate the scalar bi-spectrum and the non-Gaussianity parameter  $f_{\text{NL}}$  for single field inflationary models involving the canonical scalar field. Although, some partial numerical results have already been published in the literature, we believe that it is for the first time that a general and efficient code has been put together to evaluate the complete scalar bi-spectrum. Though, we shall largely restrict our discussion in this paper to the equilateral case, as we shall illustrate, the code can compute the scalar bi-spectrum and the parameter  $f_{\text{NL}}$  for any triangular configuration of the wavevectors. Also, as we shall demonstrate, BINGO can also compute *all* the different contributions to the bi-spectrum. Moreover, it is worth noting that, under certain conditions, the code can arrive at the results within a matter of a few minutes. We should mention here that we have made a limited version of BINGO, viz. one that focuses on the equilateral limit, available online at <https://www.physics.iitm.ac.in/~sriram/bingo/bingo.html>.

As an immediate application, we shall utilize the code to examine of the power of the non-Gaussianity parameter  $f_{\text{NL}}$  to discriminate between different inflationary models that admit deviations from slow roll and generate similar features in the scalar power spectrum. Recall that, most single field inflationary models naturally lead to an extended period of slow roll and hence to nearly scale invariant primordial power spectra (see, for example, any of the following texts [11] or reviews [12]), which seem to be fairly consistent with the recent data on the anisotropies in the Cosmic Microwave Background (CMB) (in this context, see Refs. [5, 6, 7]; for a comparison of a class of inflationary models with the data, see, for example, Ref. [13] and references therein) as well as other observational constraints. However, it has been repeatedly

noticed that certain features in the inflationary scalar power spectrum can improve the fit to the CMB data at the cost of some additional parameters (see, for instance, Refs. [14, 15, 16, 17, 18, 19, 20, 21, 22, 23, 24, 25, 26, 27, 28]). Though the statistical significance of these features remain to be understood satisfactorily [29], they gain importance from the phenomenological perspective of comparing the models with the data, because only a smaller class of single field inflationary models, which allow for departures from slow roll, can generate them. Interestingly, demanding the presence of features in the scalar power spectrum seems to generically lead to larger non-Gaussianities (see, for example, Refs. [30, 31]). Therefore, features may offer the only route (unless one works with non-vacuum initial states [32]) for the canonical scalar fields to remain viable if  $f_{\text{NL}}$  turns out to be significant.

If indeed the presence of features turns out to be the correct reason behind possibly large non-Gaussianities, can we observationally identify the correct underlying inflationary scenario, in particular, given the fact that different models can lead to similar features in the scalar power spectrum? In other words, to what extent can the non-Gaussianity parameter  $f_{\text{NL}}$  help us discriminate between the inflationary models that permit features? To address this question, we shall consider a few typical inflationary models leading to features, assuming that they can be viewed as representatives of such a class of scenarios. Concretely, we shall consider the Starobinsky model [33] and the punctuated inflationary scenario [17], both of which result in a sharp drop in power at large scales that is followed by oscillations. We shall also study large and small field models with an additional step introduced in the inflaton potential [19, 30, 31]. The step leads to a burst of oscillations in the scalar power spectrum which improve the fit to the outliers near the multipole moments of  $\ell = 22$  and 40 in the CMB anisotropies. We shall also consider oscillating inflaton potentials such as the one that arises in the axion monodromy model which lead to modulations in the power spectrum over a wide range of scales [25, 26, 27, 28].

The plan of this paper is as follows. In the following section, we shall quickly describe a few essential details pertaining to the power spectrum and the bi-spectrum as well as the non-Gaussianity parameter  $f_{\text{NL}}$  in inflationary models involving a single, canonical, scalar field. In Sec. 3, after demonstrating that the super Hubble contributions to the bi-spectrum during inflation prove to be negligible, we shall describe the method that BINGO adopts to numerically compute the bi-spectrum and the non-Gaussianity parameter  $f_{\text{NL}}$ . We shall also illustrate the extent of accuracy of BINGO by comparing the numerical results with the analytical results available in three situations. Firstly, restricting ourselves to the equilateral limit, we shall compare the results from the numerical computations with the spectral dependence of the bi-spectrum expected in power law inflation. Secondly, focusing on the case of the archetypical quadratic potential, we shall contrast the numerical results with the analytical expressions obtained using the slow roll approximation for an arbitrary triangular configuration of the wavevectors. Thirdly, considering a more non-trivial situation involving a brief period of fast roll, we shall compare the numerical results with

the analytical results that have recently been obtained in the case of the Starobinsky model in the equilateral limit [34, 35]. In the succeeding two sections, we shall utilize BINGO to examine of the power of the non-Gaussianity parameter  $f_{\text{NL}}$  to discriminate between different inflationary models that permit deviations from slow roll and generate similar features in the scalar power spectrum. After a quick outline of the inflationary models of our interest, we shall discuss the scalar power spectra that arise in these models. We shall then present the main results, and compare the  $f_{\text{NL}}$  that arise in the various models that we consider. We shall finally conclude in Sec. 6 with a brief summary and outlook.

A few words on our conventions and notations are in order before we proceed. We shall work with units such that  $c = \hbar = 1$ , and we shall set  $M_{\text{Pl}}^2 = (8\pi G)^{-1}$ . As is often done in the context of inflation, we shall assume the background to be described by the spatially flat, Friedmann-Lemaitre-Robertson-Walker line-element. We shall denote the conformal time as  $\eta$ , while  $N$  shall represent the number of e-folds. Moreover, an overprime shall denote differentiation with respect to the conformal time coordinate  $\eta$ . Lastly,  $a$  shall denote the scale factor, with the corresponding Hubble parameter being defined as  $H = a'/a^2$ .

## 2. The scalar power spectrum, bi-spectrum and the parameter $f_{\text{NL}}$

In this section, we shall first rapidly summarize the essential definitions of the power spectrum and the bi-spectrum as well as the non-Gaussianity parameter  $f_{\text{NL}}$ . We shall then list the various contributions to the bi-spectrum that arise in the Maldacena formalism (for the original discussions, see Refs. [1, 2, 3, 30, 31]; for more recent discussions, see, for example, Refs. [34, 36]).

### 2.1. Essential definitions and relations

Let us begin by recalling some essential points concerning the power spectrum. On quantization, the operator corresponding to the curvature perturbation  $\mathcal{R}(\eta, \mathbf{x})$  can be expressed as

$$\begin{aligned} \hat{\mathcal{R}}(\eta, \mathbf{x}) &= \int \frac{d^3\mathbf{k}}{(2\pi)^{3/2}} \hat{\mathcal{R}}_{\mathbf{k}}(\eta) e^{i\mathbf{k}\cdot\mathbf{x}} \\ &= \int \frac{d^3\mathbf{k}}{(2\pi)^{3/2}} \left[ \hat{a}_{\mathbf{k}} f_{\mathbf{k}}(\eta) e^{i\mathbf{k}\cdot\mathbf{x}} + \hat{a}_{\mathbf{k}}^\dagger f_{\mathbf{k}}^*(\eta) e^{-i\mathbf{k}\cdot\mathbf{x}} \right], \end{aligned} \quad (1)$$

where  $\hat{a}_{\mathbf{k}}$  and  $\hat{a}_{\mathbf{k}}^\dagger$  are the usual creation and annihilation operators that satisfy the standard commutation relations. The modes  $f_{\mathbf{k}}$  are governed by the differential equation [11, 12]

$$f_{\mathbf{k}}'' + 2 \frac{z'}{z} f_{\mathbf{k}}' + k^2 f_{\mathbf{k}} = 0, \quad (2)$$

where  $z = a M_{\text{Pl}} \sqrt{2\epsilon_1}$ , with  $\epsilon_1 = -d \ln H / dN$  being the first slow roll parameter. The dimensionless scalar power spectrum  $\mathcal{P}_{\text{s}}(k)$  is defined in terms of the correlation function

of the Fourier modes of the curvature perturbation  $\hat{\mathcal{R}}_{\mathbf{k}}$  as follows:

$$\langle 0 | \hat{\mathcal{R}}_{\mathbf{k}}(\eta) \hat{\mathcal{R}}_{\mathbf{p}}(\eta) | 0 \rangle = \frac{(2\pi)^2}{2k^3} \mathcal{P}_s(k) \delta^{(3)}(\mathbf{k} + \mathbf{p}), \quad (3)$$

where  $|0\rangle$  denotes the Bunch-Davies vacuum which is defined as  $\hat{a}_{\mathbf{k}}|0\rangle = 0 \forall \mathbf{k}$  [37]. In terms of the modes  $f_{\mathbf{k}}$ , the scalar power spectrum is given by

$$\mathcal{P}_s(k) = \frac{k^3}{2\pi^2} |f_{\mathbf{k}}|^2. \quad (4)$$

As is well known, numerically, the initial conditions are imposed on the modes  $f_{\mathbf{k}}$  when they are well inside the Hubble radius, and the power spectrum is evaluated at suitably late times when the modes are sufficiently outside the Hubble radius (see, for instance, Refs. [38]). We shall discuss the details concerning the numerical evolution of the background as well as the perturbations and the computation of the corresponding power spectrum in the next section.

The scalar bi-spectrum  $\mathcal{B}_s(\mathbf{k}_1, \mathbf{k}_2, \mathbf{k}_3)$  is related to the three point correlation function of the Fourier modes of the curvature perturbation  $\hat{\mathcal{R}}_{\mathbf{k}}$ , evaluated at the end of inflation, say, at the conformal time  $\eta_e$ , as follows [6]:

$$\langle \hat{\mathcal{R}}_{\mathbf{k}_1}(\eta_e) \hat{\mathcal{R}}_{\mathbf{k}_2}(\eta_e) \hat{\mathcal{R}}_{\mathbf{k}_3}(\eta_e) \rangle = (2\pi)^3 \mathcal{B}_s(\mathbf{k}_1, \mathbf{k}_2, \mathbf{k}_3) \delta^{(3)}(\mathbf{k}_1 + \mathbf{k}_2 + \mathbf{k}_3). \quad (5)$$

In our discussion below, for the sake of convenience, we shall set

$$\mathcal{B}_s(\mathbf{k}_1, \mathbf{k}_2, \mathbf{k}_3) = (2\pi)^{-9/2} G(\mathbf{k}_1, \mathbf{k}_2, \mathbf{k}_3). \quad (6)$$

The observationally relevant non-Gaussianity parameter  $f_{\text{NL}}$  is introduced through the relation

$$\mathcal{R}(\eta, \mathbf{x}) = \mathcal{R}_G(\eta, \mathbf{x}) - \frac{3f_{\text{NL}}}{5} [\mathcal{R}_G^2(\eta, \mathbf{x}) - \langle \mathcal{R}_G^2(\eta, \mathbf{x}) \rangle], \quad (7)$$

where  $\mathcal{R}_G$  denotes the Gaussian quantity, and the factor of  $3/5$  arises due to the relation between the Bardeen potential and the curvature perturbation during the matter dominated epoch. Upon making use of the corresponding relation between  $\mathcal{R}$  and  $\mathcal{R}_G$  in Fourier space and the Wick's theorem, one obtains that [1, 2, 3]

$$\begin{aligned} \langle \hat{\mathcal{R}}_{\mathbf{k}_1} \hat{\mathcal{R}}_{\mathbf{k}_2} \hat{\mathcal{R}}_{\mathbf{k}_3} \rangle &= -\frac{3f_{\text{NL}}}{10} (2\pi)^4 (2\pi)^{-3/2} \frac{1}{k_1^3 k_2^3 k_3^3} \delta^{(3)}(\mathbf{k}_1 + \mathbf{k}_2 + \mathbf{k}_3) \\ &\times [k_1^3 \mathcal{P}_s(k_2) \mathcal{P}_s(k_3) + \text{two permutations}]. \end{aligned} \quad (8)$$

This expression can then be utilized to arrive at the following relation between the non-Gaussianity parameter  $f_{\text{NL}}$  and the scalar bi-spectrum  $\mathcal{B}_s(\mathbf{k}_1, \mathbf{k}_2, \mathbf{k}_3)$  or, equivalently, the quantity  $G(\mathbf{k}_1, \mathbf{k}_2, \mathbf{k}_3)$  that we have introduced [34, 36]:

$$\begin{aligned} f_{\text{NL}}(\mathbf{k}_1, \mathbf{k}_2, \mathbf{k}_3) &= -\frac{10}{3} (2\pi)^{-4} (k_1 k_2 k_3)^3 G(\mathbf{k}_1, \mathbf{k}_2, \mathbf{k}_3) \\ &\times [k_1^3 \mathcal{P}_s(k_2) \mathcal{P}_s(k_3) + \text{two permutations}]^{-1}. \end{aligned} \quad (9)$$

In particular, in the equilateral limit, i.e. when  $k_1 = k_2 = k_3 = k$ , this expression simplifies to

$$f_{\text{NL}}^{\text{eq}}(k) = -\frac{10}{9} \frac{1}{(2\pi)^4} \frac{k^6 G(k)}{\mathcal{P}_s^2(k)}. \quad (10)$$

Two points need to be emphasized here regarding the above expressions for the quantities  $f_{\text{NL}}$  and  $f_{\text{NL}}^{\text{eq}}$ . Firstly, it ought to be noted that the non-Gaussianity  $f_{\text{NL}}$  parameter introduced in Eq. (7) [as well as the expression arrived at in Eq. (9)] corresponds to the so-called local form of the parameter. Secondly, the quantity  $f_{\text{NL}}^{\text{eq}}$  corresponds to the equilateral limit of the *local*  $f_{\text{NL}}$  parameter, and is intrinsically different from a similar parameter introduced when the bi-spectrum has the equilateral form (in this context, see, for instance, Ref. [7]).

## 2.2. The scalar bi-spectrum in the Maldacena formalism

In the Maldacena formalism [1], the bi-spectrum is evaluated using the standard rules of perturbative quantum field theory, based on the interaction Hamiltonian that depends cubically on the curvature perturbation. It can be shown that the bi-spectrum that results from the interaction Hamiltonian can be expressed as [1, 2, 3, 30, 31, 34, 36]

$$\begin{aligned}
 G(\mathbf{k}_1, \mathbf{k}_2, \mathbf{k}_3) &\equiv \sum_{C=1}^7 G_C(\mathbf{k}_1, \mathbf{k}_2, \mathbf{k}_3) \\
 &\equiv M_{\text{Pl}}^2 \sum_{C=1}^6 \left\{ [f_{\mathbf{k}_1}(\eta_e) f_{\mathbf{k}_2}(\eta_e) f_{\mathbf{k}_3}(\eta_e)] \mathcal{G}_C(\mathbf{k}_1, \mathbf{k}_2, \mathbf{k}_3) \right. \\
 &\quad \left. + [f_{\mathbf{k}_1}^*(\eta_e) f_{\mathbf{k}_2}^*(\eta_e) f_{\mathbf{k}_3}^*(\eta_e)] \mathcal{G}_C^*(\mathbf{k}_1, \mathbf{k}_2, \mathbf{k}_3) \right\} \\
 &\quad + G_7(\mathbf{k}_1, \mathbf{k}_2, \mathbf{k}_3). \tag{11}
 \end{aligned}$$

The quantities  $\mathcal{G}_C(\mathbf{k}_1, \mathbf{k}_2, \mathbf{k}_3)$  with  $C = (1, 6)$  correspond to the six terms in the interaction Hamiltonian, and are described by the integrals

$$\mathcal{G}_1(\mathbf{k}_1, \mathbf{k}_2, \mathbf{k}_3) = 2i \int_{\eta_i}^{\eta_e} d\eta a^2 \epsilon_1^2 (f_{\mathbf{k}_1}^* f_{\mathbf{k}_2}^* f_{\mathbf{k}_3}^* + \text{two permutations}), \tag{12}$$

$$\begin{aligned}
 \mathcal{G}_2(\mathbf{k}_1, \mathbf{k}_2, \mathbf{k}_3) &= -2i (\mathbf{k}_1 \cdot \mathbf{k}_2 + \text{two permutations}) \\
 &\quad \times \int_{\eta_i}^{\eta_e} d\eta a^2 \epsilon_1^2 f_{\mathbf{k}_1}^* f_{\mathbf{k}_2}^* f_{\mathbf{k}_3}^*, \tag{13}
 \end{aligned}$$

$$\begin{aligned}
 \mathcal{G}_3(\mathbf{k}_1, \mathbf{k}_2, \mathbf{k}_3) &= -2i \int_{\eta_i}^{\eta_e} d\eta a^2 \epsilon_1^2 \left[ \left( \frac{\mathbf{k}_1 \cdot \mathbf{k}_2}{k_2^2} \right) f_{\mathbf{k}_1}^* f_{\mathbf{k}_2}^* f_{\mathbf{k}_3}^* \right. \\
 &\quad \left. + \text{five permutations} \right], \tag{14}
 \end{aligned}$$

$$\mathcal{G}_4(\mathbf{k}_1, \mathbf{k}_2, \mathbf{k}_3) = i \int_{\eta_i}^{\eta_e} d\eta a^2 \epsilon_1 \epsilon_2' (f_{\mathbf{k}_1}^* f_{\mathbf{k}_2}^* f_{\mathbf{k}_3}^* + \text{two permutations}), \tag{15}$$

$$\begin{aligned}
 \mathcal{G}_5(\mathbf{k}_1, \mathbf{k}_2, \mathbf{k}_3) &= \frac{i}{2} \int_{\eta_i}^{\eta_e} d\eta a^2 \epsilon_1^3 \left[ \left( \frac{\mathbf{k}_1 \cdot \mathbf{k}_2}{k_2^2} \right) f_{\mathbf{k}_1}^* f_{\mathbf{k}_2}^* f_{\mathbf{k}_3}^* \right. \\
 &\quad \left. + \text{five permutations} \right], \tag{16}
 \end{aligned}$$

$$\mathcal{G}_6(\mathbf{k}_1, \mathbf{k}_2, \mathbf{k}_3) = \frac{i}{2} \int_{\eta_i}^{\eta_e} d\eta a^2 \epsilon_1^3 \left\{ \left[ \frac{k_1^2 (\mathbf{k}_2 \cdot \mathbf{k}_3)}{k_2^2 k_3^2} \right] f_{\mathbf{k}_1}^* f_{\mathbf{k}_2}^* f_{\mathbf{k}_3}^* \right.$$

$$+ \text{two permutations} \left. \vphantom{\int} \right\}, \quad (17)$$

where  $\epsilon_2$  is the second slow roll parameter that is defined with respect to the first as follows:  $\epsilon_2 = d \ln \epsilon_1 / dN$ . The lower limit of the above integrals, viz.  $\eta_i$ , denotes a sufficiently early time when the initial conditions are imposed on the modes. The additional, seventh term  $G_7(\mathbf{k}_1, \mathbf{k}_2, \mathbf{k}_3)$  arises due to the field redefinition, and its contribution to  $G(\mathbf{k}_1, \mathbf{k}_2, \mathbf{k}_3)$  is given by

$$G_7(\mathbf{k}_1, \mathbf{k}_2, \mathbf{k}_3) = \frac{\epsilon_2(\eta_e)}{2} (|f_{\mathbf{k}_2}(\eta_e)|^2 |f_{\mathbf{k}_3}(\eta_e)|^2 + \text{two permutations}). \quad (18)$$

### 3. The numerical computation of the scalar bi-spectrum

In this section, after illustrating that the super-Hubble contributions to the complete bi-spectrum during inflation proves to be negligible, we shall outline the methods that BINGO adopts to numerically evolve the equations governing the background and the perturbations, and eventually evaluate the inflationary scalar power and bi-spectra. Also, we shall illustrate the extent of accuracy of BINGO by comparing the results from the code with the expected form of the bi-spectrum in the equilateral limit in power law inflation and the analytical results that are available in the case of the Starobinsky model [34, 35]. We shall also contrast the numerical results with the analytical results obtained under the slow roll approximation in the case of the popular quadratic potential for an arbitrary triangular configuration of the wavevectors.

#### 3.1. The contributions to the bi-spectrum on super-Hubble scales

It is clear from the expressions in the previous section that the evaluation of the bi-spectrum involves integrals over the mode  $f_{\mathbf{k}}$  and its derivative  $f'_{\mathbf{k}}$  as well as the slow roll parameters  $\epsilon_1$ ,  $\epsilon_2$  and the derivative  $\epsilon'_2$ . While evaluating the power spectra, it is well known that, in single field inflationary models, it suffices to evolve the curvature perturbation from an initial time when the modes are sufficiently inside the Hubble radius to a suitably late time when the amplitude of the curvature perturbation settles down to a constant value on super-Hubble scales (see, for example, Refs. [38]). We shall illustrate that many of the contributions to the bi-spectrum prove to be negligible when the modes evolve on super-Hubble scales. Interestingly, we shall also show that, those contributions to the bi-spectrum which turn out to be significant at late times when the modes are well outside the Hubble radius are canceled by certain other contributions that arise. As a consequence, we shall argue that, numerically, it suffices to evaluate the integrals over the period of time during which the curvature perturbations have been conventionally evolved to arrive at the power spectra, viz. from the sub-Hubble to the super-Hubble scales. In fact, we had recently shown that, for cosmological modes that are on super-Hubble scales during preheating, the contributions to the bi-spectrum and, equivalently, to the non-Gaussianity parameter  $f_{\text{NL}}$ , prove to be negligible [36]. The calculations we had presented in the work can be easily extended to the case of

the modes on super-Hubble scales during inflation. Therefore, we shall rapidly sketch the essential arguments below, referring the readers to our recent work for further details [36].

*3.1.1. Evolution of  $f_{\mathbf{k}}$  on super-Hubble scales* During inflation, when the modes are on super-Hubble scales, it is well known that the solution to  $f_{\mathbf{k}}$  can be written as [11, 12]

$$f_{\mathbf{k}} \simeq A_{\mathbf{k}} + B_{\mathbf{k}} \int^{\eta} \frac{d\tilde{\eta}}{z^2(\tilde{\eta})}, \quad (19)$$

where  $A_{\mathbf{k}}$  and  $B_{\mathbf{k}}$  are  $\mathbf{k}$ -dependent constants which are determined by the initial conditions imposed on the modes in the sub-Hubble limit. The first term involving  $A_{\mathbf{k}}$  is the growing mode, which is actually a constant, while the term containing  $B_{\mathbf{k}}$  represents the decaying mode. Therefore, on super-Hubble scales, the mode  $f_{\mathbf{k}}$  simplifies to

$$f_{\mathbf{k}} \simeq A_{\mathbf{k}}. \quad (20)$$

Moreover, the leading non-zero contribution to its derivative is determined by the decaying mode, and is given by

$$f'_{\mathbf{k}} \simeq \frac{B_{\mathbf{k}}}{z^2} = \frac{\bar{B}_{\mathbf{k}}}{a^2 \epsilon_1}, \quad (21)$$

where we have set  $\bar{B}_{\mathbf{k}} = B_{\mathbf{k}}/(2 M_{\text{Pl}}^2)$ .

It is now a matter of making use of the above solutions for  $f_{\mathbf{k}}$  and  $f'_{\mathbf{k}}$  to determine the super-Hubble contributions to the bi-spectrum during inflation.

*3.1.2. The various contributions* To begin with, note that, each of the integrals  $\mathcal{G}_C(\mathbf{k}_1, \mathbf{k}_2, \mathbf{k}_3)$ , where  $C = (1, 6)$ , can be divided into two parts as follows:

$$\mathcal{G}_C(\mathbf{k}_1, \mathbf{k}_2, \mathbf{k}_3) = \mathcal{G}_C^{\text{is}}(\mathbf{k}_1, \mathbf{k}_2, \mathbf{k}_3) + \mathcal{G}_C^{\text{se}}(\mathbf{k}_1, \mathbf{k}_2, \mathbf{k}_3). \quad (22)$$

The integrals in the first term  $\mathcal{G}_C^{\text{is}}(\mathbf{k}_1, \mathbf{k}_2, \mathbf{k}_3)$  run from the earliest time (i.e.  $\eta_i$ ) when the smallest of the three wavenumbers  $k_1$ ,  $k_2$  and  $k_3$  is sufficiently inside the Hubble radius [typically corresponding to  $k/(aH) \simeq 100$ ] to the time (say,  $\eta_s$ ) when the largest of the three wavenumbers is well outside the Hubble radius [say, when  $k/(aH) \simeq 10^{-5}$ ]. Then, evidently, the second term  $\mathcal{G}_C^{\text{se}}(\mathbf{k}_1, \mathbf{k}_2, \mathbf{k}_3)$  will involve integrals which run from the latter time  $\eta_s$  to the end of inflation at  $\eta_e$  (in this context, see Fig. 1). In what follows, we shall discuss the various contributions to the bi-spectrum due to the terms  $\mathcal{G}_C^{\text{se}}(\mathbf{k}_1, \mathbf{k}_2, \mathbf{k}_3)$ . We shall show that the corresponding contribution either remains small or, when it proves to be large, it is exactly canceled by another contribution to the bi-spectrum.

Let us first focus on the fourth term  $G_4(\mathbf{k}_1, \mathbf{k}_2, \mathbf{k}_3)$  since it has often been found to lead to the largest contribution to the bi-spectrum when deviations from slow roll occur [30, 31, 34, 36]. As the slow roll parameters turn large towards the end of inflation, we can expect this term to contribute significantly at late times. However, as we shall quickly illustrate, such a late time contribution is exactly canceled by the contribution from  $G_7(\mathbf{k}_1, \mathbf{k}_2, \mathbf{k}_3)$  which arises due to the field redefinition [36]. Upon



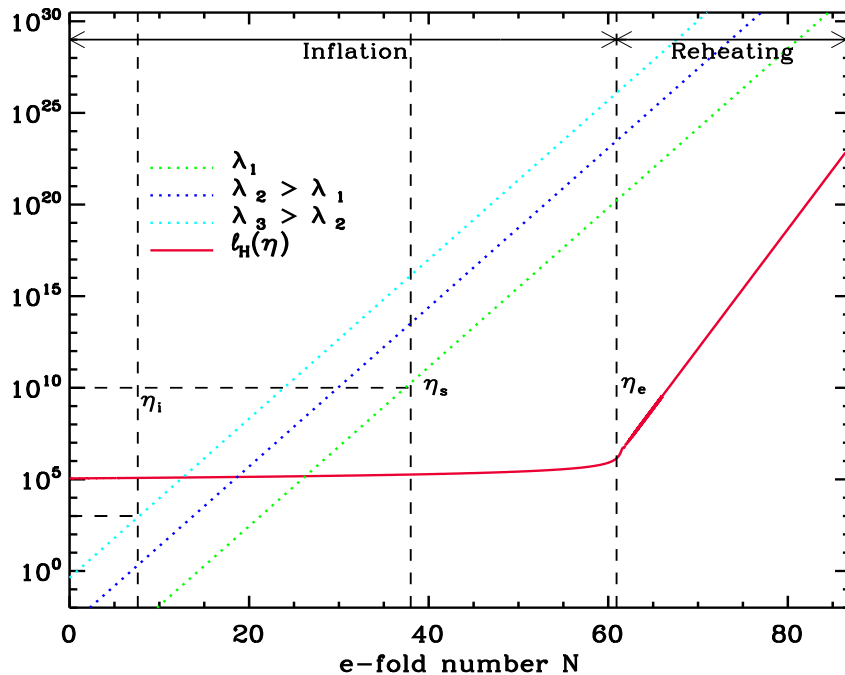


**Figure 1.** The evolution of three wavelengths, say,  $\lambda_1 < \lambda_2 < \lambda_3$  (corresponding to the wavenumbers  $k_1 > k_2 > k_3$ ) and the Hubble radius  $\ell_H = H^{-1}$  have been plotted as a function of e-folds  $N$  (in green, blue, cyan and red, respectively) during the epochs of inflation and reheating for the case of the conventional quadratic potential. Note that  $\eta_i$  corresponds to the time when the largest of the three wavelengths, viz.  $\lambda_3$  in this case, satisfies the condition  $k_3/(aH) \simeq 100$ , while  $\eta_s$  denotes the time when the smallest of the three wavelengths, i.e.  $\lambda_1$ , is sufficiently outside the Hubble radius such that, say,  $k_1/(aH) \simeq 10^{-5}$ . Inflation terminates at the time  $\eta_e$ , when the epoch of reheating is expected to begin.

using the form (20) of the mode  $f_{\mathbf{k}}$  and its derivative (21) on super-Hubble scales in the expression (15), the integral involved can be trivially carried out with the result that the corresponding contribution to the bi-spectrum can be expressed as

$$G_4^{\text{se}}(\mathbf{k}_1, \mathbf{k}_2, \mathbf{k}_3) \simeq i M_{\text{Pl}}^2 [\epsilon_2(\eta_e) - \epsilon_2(\eta_s)] \left[ |A_{\mathbf{k}_1}|^2 |A_{\mathbf{k}_2}|^2 (A_{\mathbf{k}_3} \bar{B}_{\mathbf{k}_3}^* - A_{\mathbf{k}_3}^* \bar{B}_{\mathbf{k}_3}) + \text{two permutations} \right]. \quad (23)$$

The Wronskian corresponding to the equation of motion (2) and the standard Bunch-Davies initial condition leads to the relation  $(A_{\mathbf{k}} \bar{B}_{\mathbf{k}}^* - A_{\mathbf{k}}^* \bar{B}_{\mathbf{k}}) = i/(2 M_{\text{Pl}}^2)$ , which can then be utilized to arrive at the following simpler expression [36]:

$$G_4^{\text{se}}(\mathbf{k}_1, \mathbf{k}_2, \mathbf{k}_3) \simeq -\frac{1}{2} [\epsilon_2(\eta_e) - \epsilon_2(\eta_s)] \times \left[ |A_{\mathbf{k}_1}|^2 |A_{\mathbf{k}_2}|^2 + \text{two permutations} \right]. \quad (24)$$

The first of these terms involving the value of  $\epsilon_2$  at the end of inflation *exactly* cancels the contribution  $G_7(\mathbf{k}_1, \mathbf{k}_2, \mathbf{k}_3)$  [with  $f_{\mathbf{k}}$  set to  $A_{\mathbf{k}}$  in Eq. (18)] that arises due to the

field redefinition. But, the remaining contribution cannot be ignored and needs to be taken into account. It is useful to note that this term is essentially the same as the one due to the field redefinition, but which is now evaluated on super-Hubble scales (i.e. at  $\eta_s$ ) rather than at the end of inflation. In other words, if we consider the fourth and the seventh terms together, it is equivalent to evaluating the contribution to the bi-spectrum corresponding to  $\mathcal{G}_4^{\text{is}}(\mathbf{k}_1, \mathbf{k}_2, \mathbf{k}_3)$ , and adding to it the contribution due to the seventh term  $G_7(\mathbf{k}_1, \mathbf{k}_2, \mathbf{k}_3)$  evaluated at  $\eta_s$  rather than at the end of inflation.

Let us now turn to the contribution due to the second term, which can occasionally prove to be comparable to the contribution due to the fourth term [34]. Upon making use of the behavior of the mode  $f_{\mathbf{k}}$  and its derivative on super-Hubble scales in the integral (13), one obtains the contribution to the bi-spectrum due to  $\mathcal{G}_2^{\text{se}}(\mathbf{k}_1, \mathbf{k}_2, \mathbf{k}_3)$  to be [34, 36]

$$G_2^{\text{se}}(\mathbf{k}_1, \mathbf{k}_2, \mathbf{k}_3) = -2i M_{\text{Pl}}^2 (\mathbf{k}_1 \cdot \mathbf{k}_2 + \text{two permutations}) \times |A_{\mathbf{k}_1}|^2 |A_{\mathbf{k}_2}|^2 |A_{\mathbf{k}_3}|^2 [I_2(\eta_e, \eta_s) - I_2^*(\eta_e, \eta_s)], \quad (25)$$

where the quantity  $I_2(\eta_e, \eta_s)$  is described by the integral

$$I_2(\eta_e, \eta_s) = \int_{\eta_s}^{\eta_e} d\eta a^2 \epsilon_1^2. \quad (26)$$

Note that, due to the quadratic dependence on the scale factor, actually,  $I_2(\eta_e, \eta_s)$  is a rapidly growing quantity at late times. However, the complete super-Hubble contribution to the bi-spectrum vanishes identically since the integral  $I_2(\eta_e, \eta_s)$  is a purely real quantity [36]. Hence, in the case of the second term, it is sufficient to evaluate the contribution to the bi-spectrum due to  $\mathcal{G}_2^{\text{is}}(\mathbf{k}_1, \mathbf{k}_2, \mathbf{k}_3)$ .

Due to their structure, one finds that the first and the third terms and the fifth and the sixth terms can be evaluated together. On super-Hubble scales, one can easily show that the contributions due to the first and the third terms can be written as

$$G_1^{\text{es}}(\mathbf{k}_1, \mathbf{k}_2, \mathbf{k}_3) + G_3^{\text{es}}(\mathbf{k}_1, \mathbf{k}_2, \mathbf{k}_3) = 2i M_{\text{Pl}}^2 \left[ \left( 1 - \frac{\mathbf{k}_1 \cdot \mathbf{k}_2}{k_2^2} - \frac{\mathbf{k}_1 \cdot \mathbf{k}_3}{k_3^2} \right) |A_{\mathbf{k}_1}|^2 \times (A_{\mathbf{k}_2} \bar{B}_{\mathbf{k}_2}^* A_{\mathbf{k}_3} \bar{B}_{\mathbf{k}_3}^* - A_{\mathbf{k}_2}^* \bar{B}_{\mathbf{k}_2} A_{\mathbf{k}_3}^* \bar{B}_{\mathbf{k}_3}) + \text{two permutations} \right] I_{13}(\eta_e, \eta_s), \quad (27)$$

while the corresponding contributions due to the fifth and the sixth terms can be obtained to be

$$G_5^{\text{se}}(\mathbf{k}_1, \mathbf{k}_2, \mathbf{k}_3) + G_6^{\text{se}}(\mathbf{k}_1, \mathbf{k}_2, \mathbf{k}_3) = \frac{i M_{\text{Pl}}^2}{2} \times \left[ \left( \frac{\mathbf{k}_1 \cdot \mathbf{k}_2}{k_2^2} + \frac{\mathbf{k}_1 \cdot \mathbf{k}_3}{k_3^2} + \frac{k_1^2 (\mathbf{k}_2 \cdot \mathbf{k}_3)}{k_2^2 k_3^2} \right) \times |A_{\mathbf{k}_1}|^2 \times (A_{\mathbf{k}_2} \bar{B}_{\mathbf{k}_2}^* A_{\mathbf{k}_3} \bar{B}_{\mathbf{k}_3}^* - A_{\mathbf{k}_2}^* \bar{B}_{\mathbf{k}_2} A_{\mathbf{k}_3}^* \bar{B}_{\mathbf{k}_3}) + \text{two permutations} \right] I_{56}(\eta_e, \eta_s), \quad (28)$$

where the quantities  $I_{13}(\eta_e, \eta_s)$  and  $I_{56}(\eta_e, \eta_s)$  are described by the integrals

$$I_{13}(\eta_e, \eta_s) = \int_{\eta_s}^{\eta_e} \frac{d\eta}{a^2} \quad (29)$$

and

$$I_{56}(\eta_e, \eta_s) = \int_{\eta_s}^{\eta_e} \frac{d\eta}{a^2} \epsilon_1. \quad (30)$$

Hence, the non-zero, super-Hubble contribution to the bi-spectrum is determined by the complete contribution due to the first, the third, the fifth and the sixth terms arrived at above. In order to illustrate that this contribution is insignificant, we shall now turn to estimating the amplitude of the corresponding contribution to the non-Gaussianity parameter  $f_{\text{NL}}$ .

### 3.2. An estimate of the super-Hubble contribution to the non-Gaussianity parameter

Let us restrict ourselves to the equilateral limit for simplicity. In such a case, the super-Hubble contributions due to the first, the third, the fifth and the sixth terms to the non-Gaussianity parameter  $f_{\text{NL}}$  can be obtained by substituting the quantities (27) and (28) above in the expression (10). It is straightforward to show that the corresponding  $f_{\text{NL}}$  is given by

$$f_{\text{NL}}^{\text{eq(se)}}(k) \simeq -\frac{5iM_{\text{Pl}}^2}{18} \left( \frac{A_{\mathbf{k}}^2 \bar{B}_{\mathbf{k}}^{*2} - A_{\mathbf{k}}^{*2} \bar{B}_{\mathbf{k}}^2}{|A_{\mathbf{k}}|^2} \right) \times \left[ 12 I_{13}(\eta_e, \eta_s) - \frac{9}{4} I_{56}(\eta_e, \eta_s) \right], \quad (31)$$

where we have made use of the fact that  $f_{\mathbf{k}} \simeq A_{\mathbf{k}}$  at late times in order to arrive at the power spectrum.

To estimate the above super-Hubble contribution to the non-Gaussianity parameter  $f_{\text{NL}}^{\text{eq}}$ , let us focus on inflation of the power law form. In power law inflation, the scale factor is given by

$$a(\eta) = a_1 \left( \frac{\eta}{\eta_1} \right)^{\gamma+1}, \quad (32)$$

with  $a_1$  and  $\eta_1$  being constants, while  $\gamma$  is a free index. It is useful to note that, in such a case, the first slow roll parameter is a constant, and is given by  $\epsilon_1 = (\gamma + 2)/(\gamma + 1)$ . Under these conditions, the quantity within the brackets involving  $A_{\mathbf{k}}$  and  $\bar{B}_{\mathbf{k}}$  in the expression above can be easily evaluated (in this context, see Ref. [36]) to arrive at

$$f_{\text{NL}}^{\text{eq(se)}}(k) = \frac{5}{72\pi} \left[ 12 - \frac{9(\gamma+2)}{\gamma+1} \right] \Gamma^2 \left( \gamma + \frac{1}{2} \right) 2^{2\gamma+1} (2\gamma+1) (\gamma+2) \times (\gamma+1)^{-2(\gamma+1)} \sin(2\pi\gamma) \left[ 1 - \frac{H_s}{H_e} e^{-3(N_e - N_s)} \right] \times \left( \frac{k}{a_s H_s} \right)^{-(2\gamma+1)}. \quad (33)$$

It should be mentioned that, in arriving at this expression, for convenience, we have set  $\eta_1$  to be  $\eta_s$ , which corresponds to  $a_1$  being  $a_s$ , viz. the scale factor at  $\eta_s$ . Moreover, while  $N_s$  and  $N_e$  denote the e-folds corresponding to  $\eta_s$  and  $\eta_e$ ,  $H_s$  and  $H_e$  represent the Hubble scales at these times, respectively. Recall that,  $\eta_s$  denotes the conformal time when the largest wavenumber of interest, say,  $k_s$ , is well outside the Hubble radius, i.e. when  $k_s/(aH) \simeq 10^{-5}$ . Since  $(N_e - N_s)$  is expected to be at least 40 for the smallest cosmological scale, it is clear that the factor involving  $\exp[-3(N_e - N_s)]$  can be completely neglected. Observations point to the fact that  $\gamma \lesssim -2$ . Therefore, if we further assume that  $\gamma = -(2 + \varepsilon)$ , where  $\varepsilon \simeq 10^{-2}$ , we find that the above estimate for the non-Gaussianity parameter reduces to

$$f_{\text{NL}}^{\text{eq(se)}}(k) \lesssim -\frac{5\varepsilon^2}{9} \left( \frac{k_s}{a_s H_s} \right)^3 \simeq -10^{-19}, \quad (34)$$

where, in obtaining the final value, we have set  $k_s/(a_s H_s) = 10^{-5}$ . The inequality above arises due to the fact that, for larger scales, i.e. when  $k < k_s$ ,  $k/(aH) < 10^{-5}$  at  $\eta_s$ . In models involving the canonical scalar field, the smallest values of  $f_{\text{NL}}$  are typically generated in slow roll inflationary scenarios, wherein the non-Gaussianity parameter has been calculated to be of the order of the first slow roll parameter [1, 3]. The above estimate clearly points to fact that the super-Hubble contributions to the complete bi-spectrum and the non-Gaussianity parameter  $f_{\text{NL}}$  can be entirely ignored.

In summary, to determine the scalar bi-spectrum, it suffices to evaluate the contributions to the bi-spectrum due to the quantities  $\mathcal{G}_C^{\text{is}}(\mathbf{k}_1, \mathbf{k}_2, \mathbf{k}_3)$ , with  $C = (1, 6)$ , which involve integrals running from the initial time  $\eta_i$  to the time  $\eta_s$  when the smallest of the three modes reaches super-Hubble scales (cf. Fig. 1). Further, the addition of the contribution due to the field redefinition evaluated at  $\eta_s$  ensures that no non-trivial super-Hubble contributions are ignored. In the following sub-section, with the help of a specific example, we shall also corroborate these conclusions numerically.

### 3.3. Details of the numerical methods

The scalar bi-spectrum and the parameter  $f_{\text{NL}}$  can be easily evaluated analytically in the slow roll inflationary scenario [1]. However, barring some exceptional cases [34, 35, 39], it often proves to be difficult to evaluate the bi-spectrum analytically when departures from slow roll occur. Hence, one has to resort to numerical computations in such cases.

BINGO solves the background as well as the perturbation equations using RKSUITE [40], which is a publicly available routine to solve ordinary differential equations. We shall treat the number of e-folds as the independent variable, which allows for an efficient and accurate computation. To obtain the power spectrum, we impose the standard Bunch-Davies initial conditions on the perturbations when the modes are well inside the Hubble radius, and evolve them until suitably late times. Typically, in the case of smooth inflaton potentials, it suffices to evolve the modes  $f_{\mathbf{k}}$  from an initial time when  $k/(aH) = 100$ . However, in certain models wherein the potentials contain oscillatory terms, the modes may have to be evolved from deeper

inside the Hubble radius. For example, in the case of the axion monodromy model that we shall discuss in due course (see Sub-sec. 4.2), for values of the model parameters of our interest, we find that we need to evolve the modes from an initial time when  $k/(aH) \simeq 250$ , so that the resonance that occurs in the model due to the oscillations in the potential is captured [26, 28, 30, 31]. The scalar power spectra that arise in the various models of our interest, as displayed in Fig. 9, have all been evaluated at super-Hubble scales, say, when  $k/(aH) \simeq 10^{-5}$ , which is typically when the amplitude of the curvature perturbations freeze in.

Having obtained the behavior of the background and the modes, BINGO carries out the integrals involved in arriving at the bi-spectrum using the method of adaptive quadrature [41]. It is useful to note that, in the equilateral limit of the bi-spectrum, which we shall largely concentrate on in this work, we can evolve each of the modes of interest independently and calculate the integrals for the modes separately. The integrals  $\mathcal{G}_n$  actually contain a cut off in the sub-Hubble limit, which is essential for singling out the perturbative vacuum [1, 2, 3]. Numerically, the presence of the cut off is fortunate since it controls the contributions due to the continuing oscillations that would otherwise occur. We should highlight here that such a cut off procedure was originally introduced in the earliest numerical efforts to evaluate the scalar bi-spectrum in situations involving deviations from slow roll (in this context, see Refs. [30]). Generalizing the cut off that is often introduced analytically in the slow roll case, we shall impose a cut off of the form  $\exp[-\kappa k/(aH)]$ , where  $\kappa$  is a small parameter. In the previous two sub-sections, we had discussed as to how the integrals need to be carried out from the early time  $\eta_i$  when the largest scale is well inside the Hubble radius to the late time  $\eta_s$  when the smallest scale is sufficiently outside. If one is focusing on the equilateral configuration, rather than integrate from  $\eta_i$  to  $\eta_s$ , it suffices to compute the integrals for the modes from the time when each of them satisfy the sub-Hubble condition, say,  $k/(aH) = 100$ , to the time when they are well outside the Hubble radius, say, when  $k/(aH) = 10^{-5}$ . In other words, one carries out the integrals exactly over the period the modes are evolved to obtain the power spectrum. The presence of the cut-off ensures that the contributions at early times, i.e. near  $\eta_i$ , are negligible. Furthermore, it should be noted that, in such a case, the corresponding super-Hubble contribution to  $f_{\text{NL}}^{\text{eq}}$  will saturate the bound (34) in power law inflation for all the modes.

With the help of a specific example, let us now illustrate that, for a judicious choice of  $\kappa$ , the results from BINGO are largely independent of the upper and the lower limits of the integrals. In fact, working in the equilateral limit, we shall demonstrate these points in two steps for the case of the standard quadratic potential [see Eq. (46)]. Firstly, focusing on a specific mode, we shall fix the upper limit of the integral to be the time when  $k/(aH) = 10^{-5}$ . Evolving the mode from different initial times, we shall evaluate the integrals involved from these initial times to the fixed final time for different values of  $\kappa$ . This exercise helps us to identify an optimal value for  $\kappa$  when we shall eventually carry out the integrals from  $k/(aH) = 100$ . Secondly, upon choosing the optimal value for  $\kappa$  and integrating from  $k/(aH) = 100$ , we shall calculate the integrals for different

upper limits. For reasons outlined in the previous two sub-sections, it proves to be necessary to consider the contributions to the bi-spectrum due to the fourth and the seventh terms together. Moreover, since the first and the third, and the fifth and the sixth, have similar structure in the equilateral limit, it turns out to be convenient to club these terms as we have discussed before. In Fig. 2, we have plotted the value of  $k^6$  times the different contributions to the bi-spectrum, viz.  $G_1 + G_3$ ,  $G_2$ ,  $G_4 + G_7$  and  $G_5 + G_6$ , as a function of  $\kappa$  when the integrals have been carried out from  $k/(aH)$  of  $10^2$ ,  $10^3$  and  $10^4$  for a mode which leaves the Hubble radius around 53 e-folds before the end of inflation in the case of the quadratic potential. The figure suggests that the term  $G_4 + G_7$  is fairly independent of the cut-off parameter  $\kappa$ . This can be attributed to the fact that the integral  $\mathcal{G}_4$  depends on the quantity  $\epsilon'_2$ , which effectively behaves as a cut off. For this reason, actually, we shall *not* introduce the cut off while evaluating the term  $G_4$ . Moreover, the figure clearly indicates  $\kappa = 0.1$  to be a highly suitable value for the other terms. A larger  $\kappa$  leads to a sharper cut off reducing the value of the integrals. One could work with a smaller  $\kappa$ , in which case, the figure suggests that, one would also need to necessarily integrate from deeper inside the Hubble radius. In Fig. 3, after fixing  $\kappa$  to be 0.1 and, with the initial conditions imposed at  $k/(aH) = 10^2$ , we have plotted the four contributions to the bi-spectrum for a mode that leaves the Hubble radius at 50 e-folds before the end of inflation as a function of the upper limit of the integrals. It is evident from the figure that the values of the integrals converge quickly once the mode leave the Hubble radius. For efficient numerical integration, as in the case of the power spectrum, we have chosen the super-Hubble limit to correspond to  $k/(aH) = 10^{-5}$ . We have repeated similar tests for the other models of our interest too. These tests confirm the conclusions that we have arrived at above, indicating the robustness of the numerical methods and procedures that we have adopted. It is important that we stress three points further at this stage of our discussion. Firstly, in situations involving departures from slow roll, the dominant contribution, viz. the  $G_4 + G_7$  term, does not require the introduction of the cut off at all. Secondly, in the absence of analytical expressions to compare the numerical results with, it is imperative that a suitable value for the cut off parameter  $\kappa$  is arrived at by repeating the exercise that we have carried out in Fig. 2 for the specific model of interest. In this context, it is further important to appreciate the fact that the integrals involved will depend on both the cut off parameter  $\kappa$  as well as the initial value of  $k/(aH)$ . A complete check seems to be mandatory in order to ensure that a unique result is arrived at. (As we mentioned above, we have indeed carried out this exercise for the models that we consider here.) Lastly, we also need to emphasize that the above comments and conclusions would not apply to certain special cases wherein the amplitude of the curvature perturbation can evolve on super-Hubble scales such as, say, in ultra slow roll inflation (in this context, see, for instance, Ref. [42]).

Before we go on to consider the bi-spectra generated in the inflationary models of our interest, in order to demonstrate the accuracy of BINGO, we shall compare the numerical results from the code with the analytical results that can be arrived at in three

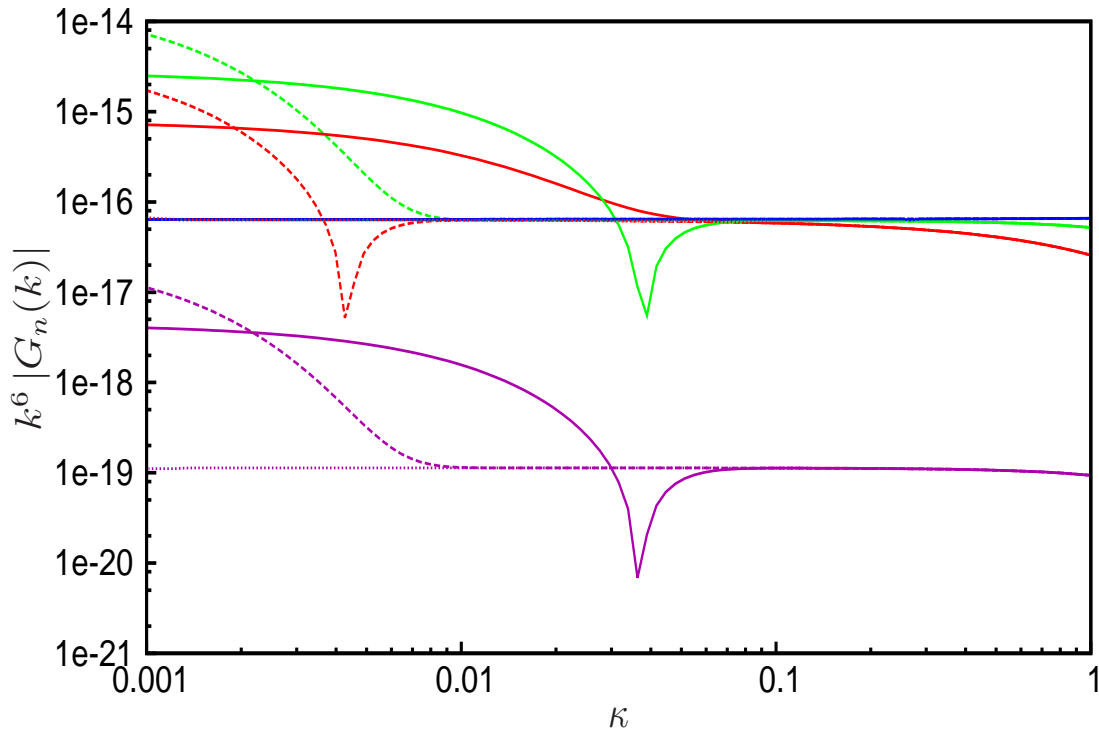


**Figure 2.** The quantities  $k^6$  times the absolute values of  $G_1 + G_3$  (in green),  $G_2$  (in red),  $G_4 + G_7$  (in blue) and  $G_5 + G_6$  (in purple) have been plotted as a function of the cut off parameter  $\kappa$  for a given mode in the case of the conventional, quadratic inflationary potential. Note that these values have been arrived at with a fixed upper limit [viz. corresponding to  $k/(aH) = 10^{-5}$ ] for the integrals involved. The solid, dashed and the dotted lines correspond to integrating from  $k/(aH)$  of  $10^2$ ,  $10^3$  and  $10^4$ , respectively. It is clear that the results converge for  $\kappa = 0.1$ , which suggests it to be an optimal value. While evaluating the bi-spectrum for the other models, we shall choose to work with a  $\kappa$  of 0.1, and impose the initial conditions as well as carry out the integrals from  $k/(aH)$  of  $10^2$  (barring the case of the axion monodromy model, as we have discussed in the text). An additional point that is worth noticing is the fact the term  $G_4 + G_7$  seems to be hardly dependent of the cut-off parameter  $\kappa$ . This can possibly be attributed to the dependence of  $G_4$  on  $\epsilon'_2$ , which can be rather small during slow roll, thereby effectively acting as a cut off. Due to this reason, hereafter, we shall not introduce the cut-off while calculating  $G_4$ .

situations. In the following sub-sections, we shall compare the results from BINGO with: (i) the spectral dependence that can be arrived at in the context of power law inflation in the equilateral limit, (ii) the slow roll results as applied to the case of the conventional quadratic potential for a generic triangular configuration of the wavevectors, and (iii) the analytic results that can be obtained for the Starobinsky model in the equilateral limit.

### 3.4. Comparison with the analytical results in the case of power law inflation

The first case that we shall discuss is power law inflation wherein, as we shall soon outline, the spectral shape of the non-zero contributions to the bi-spectrum can be

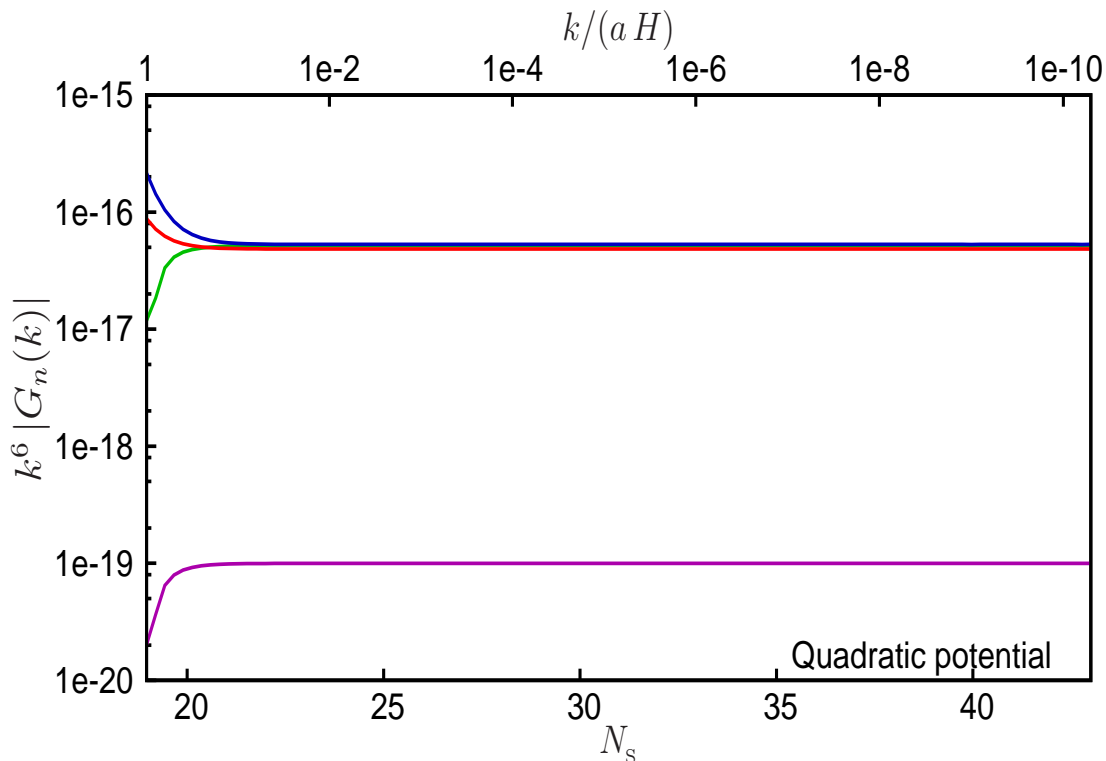


**Figure 3.** The quantities  $k^6$  times the absolute values of  $G_1 + G_3$ ,  $G_2$ ,  $G_4 + G_7$  and  $G_5 + G_6$  have been plotted (with the same choice of colors as in the previous figure) as a function of the upper limit of the integrals involved for a given mode in the case of the quadratic potential. Evidently, the integrals converge fairly rapidly to their final values once the mode leaves the Hubble radius. The independence of the results on the upper limit support the conclusions that we had earlier arrived at analytically in the last sub-section, viz. that the super-Hubble contributions to the bi-spectrum are entirely negligible. Another point that we should stress here is the fact that, since the quadratic potential only admits slow inflation, it is the  $G_7$  term that dominates in the combination  $G_4 + G_7$ .

easily arrived at in the equilateral limit.

Consider the case of power law inflation described by the scale factor (32) with  $\gamma \leq -2$ . In such a case, as we have seen,  $\epsilon_1$  is a constant and, hence,  $\epsilon_2$  and  $\epsilon_2'$ , which involve derivatives of  $\epsilon_1$ , reduce to zero. Since the contributions due to the fourth and the seventh terms, viz.  $G_4(k)$  and  $G_7(k)$ , depend on  $\epsilon_2'$  and  $\epsilon_2$ , respectively [cf. Eqs. (15) and (18)], these terms vanish identically in power law inflation. As is well known, one can express the modes  $f_{\mathbf{k}}$  as  $v_{\mathbf{k}}/z$ , where  $v_{\mathbf{k}}$  is the Mukhanov-Sasaki variable. In power law inflation, one finds that, the variable  $v_{\mathbf{k}}$  depends only on the combination  $k\eta$  (see, for example, Ref. [36]). Moreover, since  $\epsilon_1$  is a constant in power law expansion, we have  $f_{\mathbf{k}} \propto v_{\mathbf{k}}/a$ . Under these conditions, in the equilateral limit, with a simple rescaling of the variable of integration in the expressions (12), (13), (14), (16) and (17), it is straightforward to show that the quantities  $\mathcal{G}_1$ ,  $\mathcal{G}_2$ ,  $\mathcal{G}_3$ ,  $\mathcal{G}_5$  and  $\mathcal{G}_6$ , all depend on the wavenumber as  $k^{\gamma+1/2}$ . Then, upon making use of the asymptotic form of the modes  $f_{\mathbf{k}}$ , it is easy to illustrate that the corresponding contributions to the bi-spectrum,



viz.  $G_1 + G_3$ ,  $G_2$  and  $G_5 + G_6$ , all behave as  $k^{2(2\gamma+1)}$ . Since the power spectrum in power law inflation is known to have the form  $k^{2(\gamma+2)}$  (see, for example, Refs. [43]), the expression (10) for  $f_{\text{NL}}^{\text{eq}}$  then immediately suggests that the quantity will be strictly scale invariant for all  $\gamma$ . In fact, apart from these results, it is also simple to establish the following relation between the different contributions:  $G_5 + G_6 = -(3\epsilon_1/16)(G_1 + G_3)$ , a result, which, in fact, also holds in slow roll inflation [34]. In other words, in power law inflation, it is possible to arrive at the spectral dependence of the non-zero contributions to the bi-spectrum without having to explicitly calculate the integrals involved. Further, one can establish that the non-Gaussianity parameter  $f_{\text{NL}}^{\text{eq}}$  is exactly scale independent for any value of  $\gamma$ . While these arguments do not help us in determining the amplitude of the various contributions to the bi-spectrum or the non-Gaussianity parameter, their spectral shape and the relative magnitude of the above-mentioned terms provide crucial analytical results to crosscheck our numerical code. In Fig. 4, we have plotted the different non-zero contributions to the bi-spectrum computed using our numerical code and the spectral dependence we have arrived at above analytically for two different values of  $\gamma$  in the case of power law inflation. We have also indicated the relative magnitude of the first and the third and the fifth and the sixth terms arrived at numerically. Lastly, we have also illustrated the scale independent behavior of the non-Gaussianity parameter  $f_{\text{NL}}^{\text{eq}}$  for both the values of  $\gamma$ . It is clear from the figure that the numerical results agree well with the results and conclusions that we arrived at above analytically.

### 3.5. Comparison for an arbitrary triangular configuration

Let us now turn to the example of the conventional quadratic potential. The bi-spectrum in such a case can be evaluated analytically in the slow roll approximation for an arbitrary triangular configuration of the wavevectors [1, 2, 3]. In the slow roll limit, one finds that, the contributions due to the first, the second, the third and the seventh terms are of the same order, while the remaining terms turn out to be comparatively insignificant. For convenience, let us explicitly write down the contributions to the bi-spectrum due to the first, the second, the third and the seventh terms arrived at in the slow roll approximation. They are given by

$$G_1(\mathbf{k}_1, \mathbf{k}_2, \mathbf{k}_3) = \frac{H_1^4}{16 M_{\text{Pl}}^4 \epsilon_1} \left( \frac{1}{k_1 k_2 k_3} \right)^3 \times \left[ \left( 1 + \frac{k_1}{k_T} \right) \frac{k_2^2 k_3^2}{k_T} + \text{two permutations} \right], \quad (35)$$

$$G_2(\mathbf{k}_1, \mathbf{k}_2, \mathbf{k}_3) = \frac{H_1^4}{16 M_{\text{Pl}}^4 \epsilon_1} \left( \frac{1}{k_1 k_2 k_3} \right)^3 (\mathbf{k}_1 \cdot \mathbf{k}_2 + \text{two permutations}) \times \left[ -k_T + \frac{1}{k_T} (k_1 k_2 + k_1 k_3 + k_2 k_3) + \frac{k_1 k_2 k_3}{k_T^2} \right], \quad (36)$$

$$G_3(\mathbf{k}_1, \mathbf{k}_2, \mathbf{k}_3) = -\frac{H_1^4}{16 M_{\text{Pl}}^4 \epsilon_1} \left( \frac{1}{k_1 k_2 k_3} \right)^3 \left[ (\mathbf{k}_1 \cdot \mathbf{k}_2) \frac{k_3^2}{k_T} \left( 2 + \frac{k_1 + k_2}{k_T} \right) \right]$$

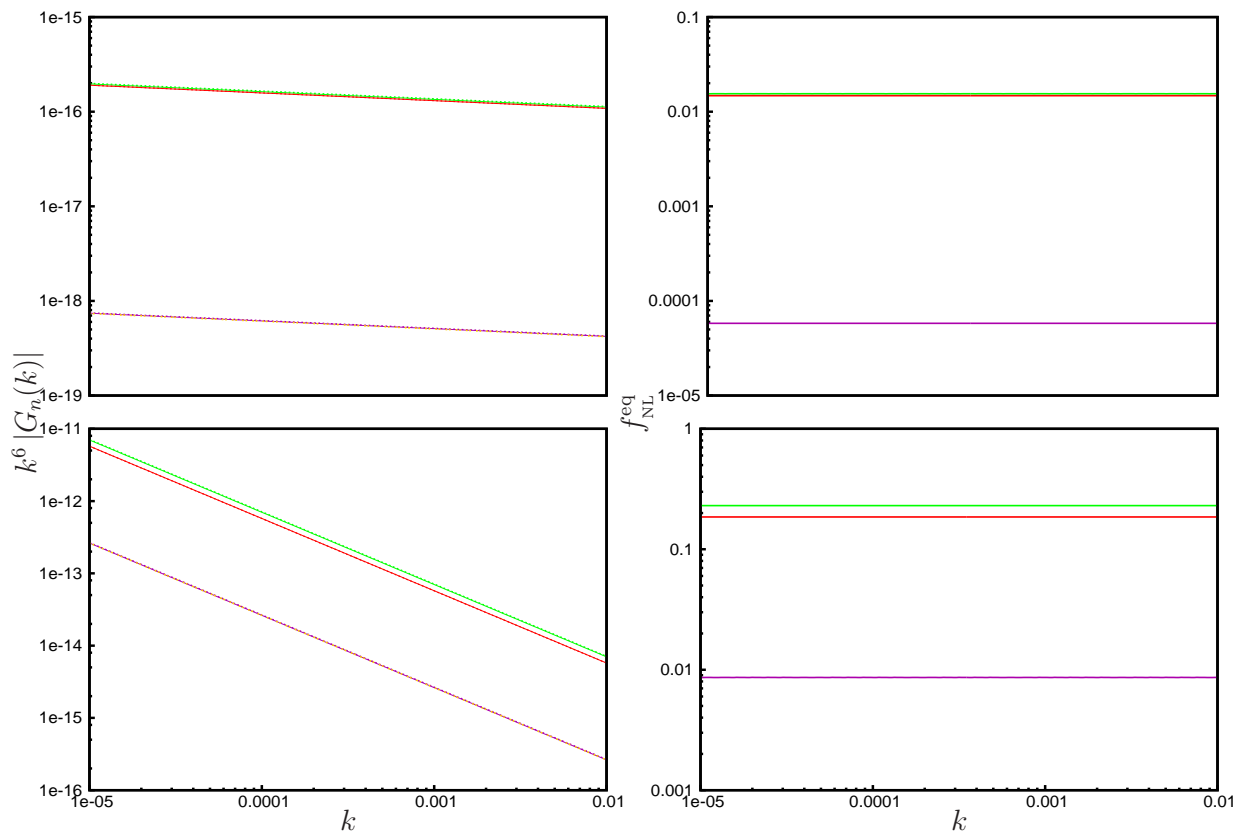


**Figure 4.** The quantities  $k^6$  times the absolute values of the non-zero contributions in the power law case, viz.  $G_1 + G_3$ ,  $G_2$  and  $G_5 + G_6$ , obtained numerically, have been plotted on the left for two different values of  $\gamma$  ( $\gamma = -2.02$  on top and  $\gamma = -2.25$  below), as solid curves with the same choice of colors to represent the different quantities as in the previous two figures. The dots on these curves are the spectral shape arrived at from the analytical arguments, with the amplitudes chosen to match the numerical results at a specific wavenumber. The dots of a different color on the solid purple curves represents  $G_5 + G_6$  obtained from its relation to  $G_1 + G_3$  discussed in the text. The plots on the right are the non-Gaussianity parameter  $f_{\text{NL}}^{\text{eq}}$  associated with the different contributions, arrived at using the numerical code. We should mention that we have also arrived at these results independently using a Mathematica [44] code. Note that, as indicated by the analytical arguments, the quantity  $f_{\text{NL}}^{\text{eq}}$  corresponding to all the contributions turns out to be strictly scale invariant for both values of  $\gamma$ .

$$\left. \begin{aligned} & + \text{two permutations} \end{aligned} \right], \quad (37)$$

$$\begin{aligned} G_7(\mathbf{k}_1, \mathbf{k}_2, \mathbf{k}_3) &= 2 \pi^4 \epsilon_2 \left( \frac{1}{k_1 k_2 k_3} \right)^3 \\ &\times [k_1^3 \mathcal{P}_s(k_2) \mathcal{P}_s(k_3) + \text{two permutations}], \end{aligned} \quad (38)$$

respectively, with  $k_{\text{T}} = k_1 + k_2 + k_3$ . The quantities  $\epsilon_1$  and  $\epsilon_2$  are the first two slow roll parameters which are assumed to be largely constant, while  $H_{\text{I}}$  denotes the Hubble scale during slow roll inflation. The scalar power spectrum during slow roll can be written

as [11, 12]

$$\mathcal{P}_s(k) = \frac{H_1^2}{8 \pi^2 M_{\text{Pl}}^2 \epsilon_1} \left( \frac{k}{k_*} \right)^{n_s - 1}, \quad (39)$$

where  $n_s = 1 - 2\epsilon_1 - \epsilon_2$  and  $k_*$  denotes a suitable, so-called, pivot scale.

From the above expressions and, upon using the fact that  $\mathbf{k}_1 + \mathbf{k}_2 + \mathbf{k}_3$  has to be zero, one can arrive at the corresponding non-Gaussianity parameter  $f_{\text{NL}}$  for an arbitrary triangular configuration of the wavevectors. We find that it can be written as

$$\begin{aligned} f_{\text{NL}}(\mathbf{k}_1, \mathbf{k}_2, \mathbf{k}_3) = & -\frac{5}{6} \left( \frac{k_1}{k_*} \right)^{-2(n_s-1)} \left[ \left( \frac{k_2}{k_1} \right)^{n_s-1} \left( \frac{k_3}{k_1} \right)^{n_s-1} \right. \\ & + \left. \left( \frac{k_2}{k_1} \right)^3 \left( \frac{k_3}{k_1} \right)^{n_s-1} + \left( \frac{k_3}{k_1} \right)^3 \left( \frac{k_2}{k_1} \right)^{n_s-1} \right]^{-1} \\ & \times \left[ \epsilon_1 \mathcal{F}_1(\mathbf{k}_1, \mathbf{k}_2, \mathbf{k}_3) + \frac{\epsilon_1}{2} \mathcal{F}_2(\mathbf{k}_1, \mathbf{k}_2, \mathbf{k}_3) \right. \\ & \left. - \frac{\epsilon_1}{2} \mathcal{F}_3(\mathbf{k}_1, \mathbf{k}_2, \mathbf{k}_3) + \frac{\epsilon_2}{2} \mathcal{F}_7(\mathbf{k}_1, \mathbf{k}_2, \mathbf{k}_3) \right], \quad (40) \end{aligned}$$

with

$$\begin{aligned} \mathcal{F}_1(\mathbf{k}_1, \mathbf{k}_2, \mathbf{k}_3) = & \left( 1 + \frac{k_2}{k_1} + \frac{k_3}{k_1} \right)^{-1} \\ & \times \left\{ \left( \frac{k_2}{k_1} \right)^2 + \left( \frac{k_3}{k_1} \right)^2 + \left( \frac{k_2}{k_1} \right)^2 \left( \frac{k_3}{k_1} \right)^2 \right. \\ & + \left. \left( 1 + \frac{k_2}{k_1} + \frac{k_3}{k_1} \right)^{-1} \right. \\ & \left. \times \left[ \frac{k_2}{k_1} \left( \frac{k_3}{k_1} \right)^2 + \frac{k_3}{k_1} \left( \frac{k_2}{k_1} \right)^2 + \left( \frac{k_2}{k_1} \right)^2 \left( \frac{k_3}{k_1} \right)^2 \right] \right\}, \quad (41) \end{aligned}$$

$$\begin{aligned} \mathcal{F}_2(\mathbf{k}_1, \mathbf{k}_2, \mathbf{k}_3) = & \left[ 1 + \left( \frac{k_2}{k_1} \right)^2 + \left( \frac{k_3}{k_1} \right)^2 \right] \\ & \times \left[ 1 + \frac{k_2}{k_1} + \frac{k_3}{k_1} \right. \\ & - \left. \left( 1 + \frac{k_2}{k_1} + \frac{k_3}{k_1} \right)^{-1} \left( \frac{k_2}{k_1} + \frac{k_3}{k_1} + \frac{k_2}{k_1} \frac{k_3}{k_1} \right) \right. \\ & \left. - \left( 1 + \frac{k_2}{k_1} + \frac{k_3}{k_1} \right)^{-2} \frac{k_2}{k_1} \frac{k_3}{k_1} \right], \quad (42) \end{aligned}$$

$$\begin{aligned} \mathcal{F}_3(\mathbf{k}_1, \mathbf{k}_2, \mathbf{k}_3) = & \left( 1 + \frac{k_2}{k_1} + \frac{k_3}{k_1} \right)^{-1} \\ & \times \left\{ \left[ 2 + \left( 1 + \frac{k_2}{k_1} + \frac{k_3}{k_1} \right)^{-1} \left( \frac{k_2}{k_1} + \frac{k_3}{k_1} \right) \right] \right. \\ & \left. \times \left[ 1 - \left( \frac{k_2}{k_1} \right)^2 - \left( \frac{k_3}{k_1} \right)^2 \right] \right\} \end{aligned}$$

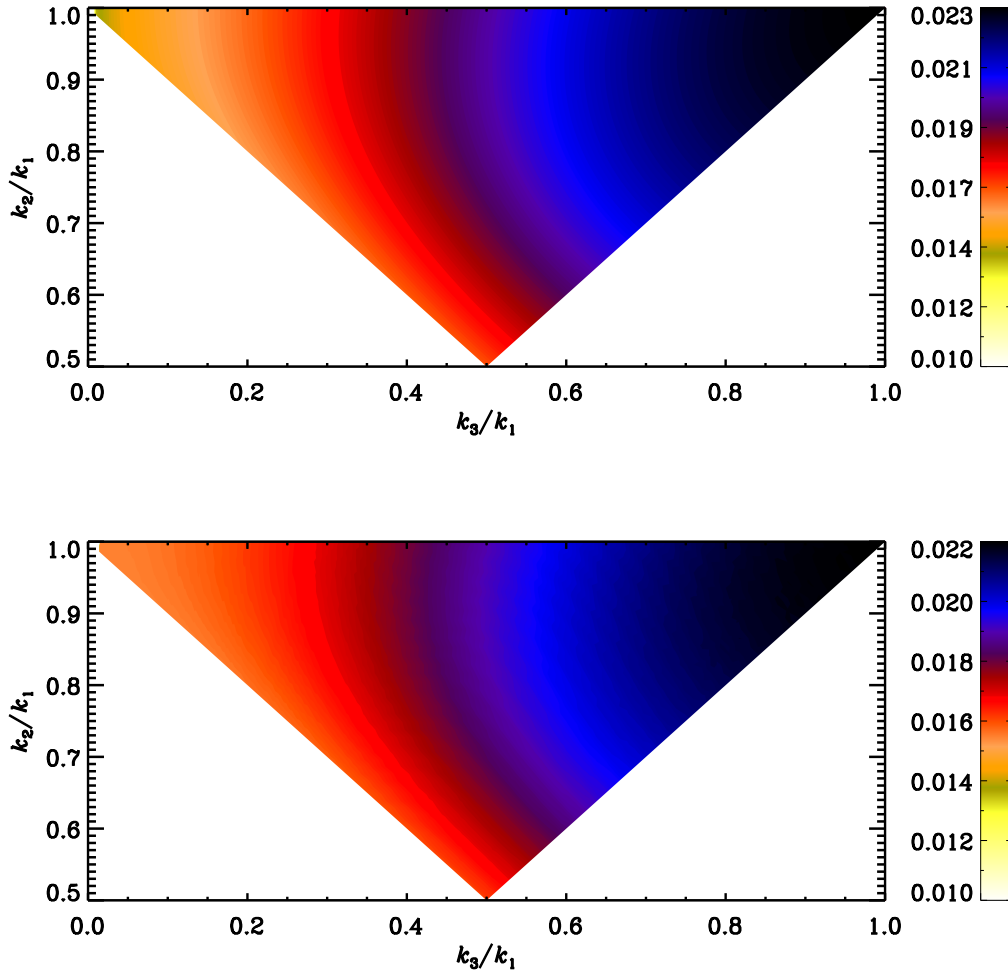


**Figure 5.** The non-Gaussianity parameter  $f_{\text{NL}}$  arising in the case of inflation driven by the archetypical quadratic potential has been plotted for an arbitrary triangular configuration of the wavevectors. The figure on top corresponds to the analytical expression that has been arrived at using the slow roll approximation, whereas the figure below represents the numerical result from BINGO. While the analytical result represents the sum of the contributions due to the first, the second, the third and the seventh terms [cf. Eqs. (35)–(38)], the numerical result takes into account the contributions due to *all* the seven terms. The two figures are strikingly similar. It should be mentioned here that the ranges of dimensionless ratios of the wavenumbers  $k_3/k_1$  and  $k_2/k_1$  for which the parameter  $f_{\text{NL}}$  have been plotted is sufficient to reveal the complete structure (in this context, see, for instance, Fig. 3 of the last reference in Refs. [9]). Also, note that we have set  $k_1 = k_*$  in arriving at the above figures.

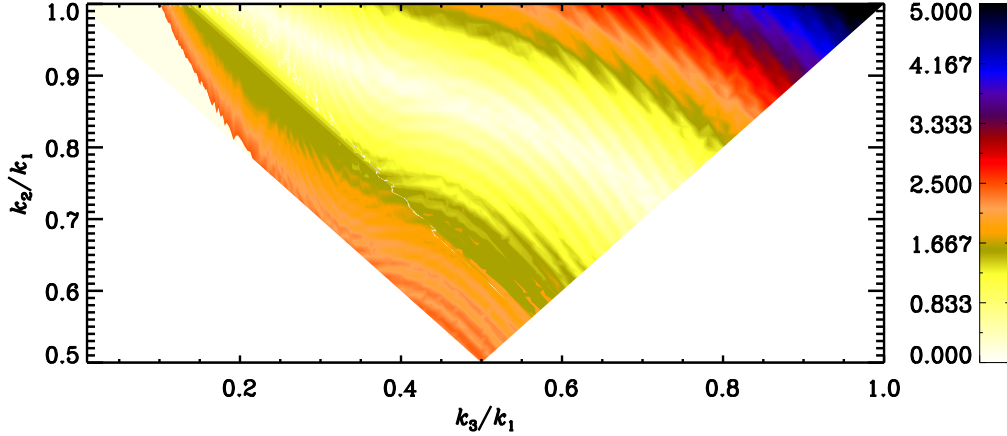


**Figure 6.** The difference in percentage between the analytical and the numerical results in the previous figure. Clearly, the maximum difference is about 5%, indicating a rather good agreement. Needless to add, BINGO seems to be performing rather well.

$$\begin{aligned}
 & - \left[ 2 + \left( 1 + \frac{k_2}{k_1} + \frac{k_3}{k_1} \right)^{-1} \left( 1 + \frac{k_2}{k_1} \right) \right] \\
 & \times \left[ 1 + \left( \frac{k_2}{k_1} \right)^2 - \left( \frac{k_3}{k_1} \right)^2 \right] \left( \frac{k_3}{k_1} \right)^2 \\
 & - \left[ 2 + \left( 1 + \frac{k_2}{k_1} + \frac{k_3}{k_1} \right)^{-1} \left( 1 + \frac{k_3}{k_1} \right) \right] \\
 & \times \left[ 1 - \left( \frac{k_2}{k_1} \right)^2 + \left( \frac{k_3}{k_1} \right)^2 \right] \left( \frac{k_2}{k_1} \right)^2 \Big\}, \quad (43)
 \end{aligned}$$

$$\begin{aligned}
 \mathcal{F}_7(\mathbf{k}_1, \mathbf{k}_2, \mathbf{k}_3) = & \left( \frac{k_1}{k_*} \right)^{2(n_S-1)} \left[ \left( \frac{k_2}{k_1} \right)^{n_S-1} \left( \frac{k_3}{k_1} \right)^{n_S-1} \right. \\
 & \left. + \left( \frac{k_2}{k_1} \right)^3 \left( \frac{k_3}{k_1} \right)^{n_S-1} + \left( \frac{k_3}{k_1} \right)^3 \left( \frac{k_2}{k_1} \right)^{n_S-1} \right]. \quad (44)
 \end{aligned}$$

In Fig. 5, we have plotted the above analytical expression for  $f_{\text{NL}}$  in the case of the quadratic potential as well as the corresponding numerical result from BINGO for an arbitrary triangular configuration of the wavevectors [9]. The two plots look remarkably alike. Also, in Fig. 6, we have plotted the percentage difference between the analytical and the numerical results. The figure suggests that the analytical and the numerical results match within 5%. It is worth stressing that part of the difference can be attributed to the slow roll approximation utilized in arriving at the analytical result. The

extent of the agreement reflects the fact that BINGO performs rather well. However, we should stress here that the level of accuracy of BINGO can be improved by essentially carrying out the integrals from a larger initial value of  $k/(aH)$  (i.e. from an earlier point in time) and simultaneously working with a smaller value of the cut off parameter  $\kappa$ .

### 3.6. Comparison in the case of the Starobinsky model

The last of the examples that we shall discuss is the Starobinsky model which involves a linear potential with a sharp change in its slope [cf. Eq. (52)]. In the Starobinsky model, under certain conditions, the complete scalar bi-spectrum can be evaluated analytically in the equilateral limit [34, 35].

As we shall discuss in the next section, in the Starobinsky model, the change in the slope causes a brief period of fast roll, which leads to sharp features in the scalar power spectrum (see Fig. 9). It was known that, for certain range of parameters, one could evaluate the scalar power spectrum analytically in the Starobinsky model, which matches the actual, numerically computed spectrum exceptionally well [33, 34]. Interestingly, it has been recently shown that, in the equilateral limit, the model allows the analytic evaluation of the complete scalar bi-spectrum too [34, 35]. In Fig. 7, we have plotted the numerical as well as the analytical results for the functions  $G_1 + G_3$ ,  $G_2$ ,  $G_4 + G_7$ , and  $G_5 + G_6$  for the Starobinsky model. We have plotted for parameters of the model for which the analytical results are considered to be a good approximation [34]. It is evident from the figure that the numerical results match the analytical ones very well. Importantly, the agreement proves to be excellent in the case of the dominant contribution  $G_4 + G_7$ . A couple of points concerning the numerical results in the case of the Starobinsky model (both in Fig. 9 wherein we have plotted the power spectrum as well as in Fig. 7 which contains the bi-spectrum) require some clarification. The second (and higher) derivatives of the potential (52) evidently contain a discontinuity. These discontinuities need to be smoothed in order for the problem to be numerically tractable. The spectra and the bi-spectra in the Starobinsky model we have illustrated have been computed with a suitable smoothing of the discontinuity, while at the same time retaining a sufficient level of sharpness so that they closely correspond to the analytical results that have been arrived at [34, 35].

## 4. The inflationary models of our interest and the resulting power spectra

In the remainder of this paper, as an immediate application, we shall utilize BINGO to examine the power of the non-Gaussianity parameter  $f_{\text{NL}}$  to help us discriminate between inflationary models that lead to similar features at the level of the scalar power spectrum. We shall list the various inflationary models of our interest in this section, and describe the power spectra that arise in these models. In the next section, we shall present the essential results and compare the  $f_{\text{NL}}$  generated in the different models.

Broadly, the models that we shall consider can be categorized into three classes.

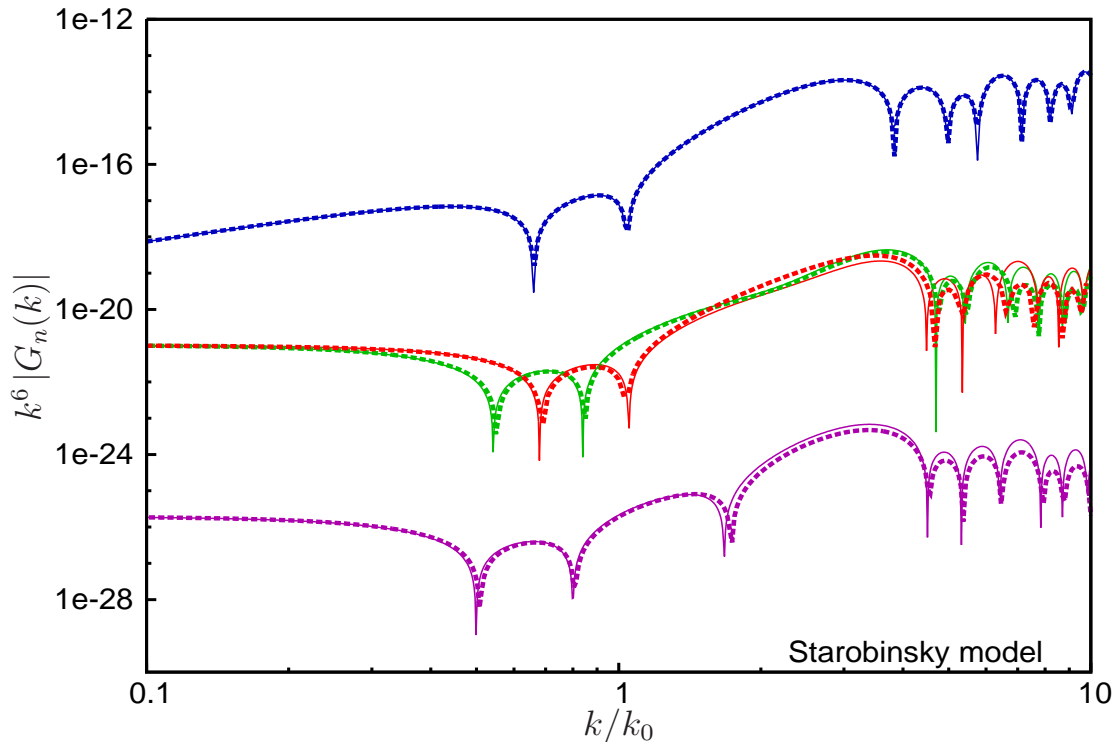


**Figure 7.** The quantities  $k^6$  times the absolute values of  $G_1 + G_3$  (in green),  $G_2$  (in red),  $G_4 + G_7$  (in blue) and  $G_5 + G_6$  (in purple) have been plotted as a function of  $k/k_0$  for the Starobinsky model. These plots correspond to the following values of the model parameters:  $V_0 = 2.36 \times 10^{-12} M_{\text{Pl}}^4$ ,  $A_+ = 3.35 \times 10^{-14} M_{\text{Pl}}^3$ ,  $A_- = 7.26 \times 10^{-15} M_{\text{Pl}}^3$  and  $\phi_0 = 0.707 M_{\text{Pl}}$ . Note that  $k_0$  is the wavenumber which leaves the Hubble radius when the scalar field crosses the break in the potential at  $\phi_0$ . The solid curves represent the analytical expressions that have been obtained recently [34, 35], while the dashed curves denote the numerical results computed using our Fortran code. We find that the numerical results match the analytical results exceptionally well (they differ by less than 1%) in the case of the crucial, dominant contribution to the  $f_{\text{NL}}$ , viz. due to  $G_4 + G_7$ .

The first class shall involve potentials which admit a relatively mild and brief departure from slow roll. The second class shall contain small but repeated deviations from slow roll, while the third and the last class shall involve a short but rather sharp departure from slow roll. Let us now briefly outline the different inflationary models that we shall consider under these classes and discuss the scalar power spectra that are generated by them.

#### 4.1. Inflationary potentials with a step

Under the first class, we shall consider models wherein a step has been introduced in potentials that otherwise admit only slow roll. Given a potential, say,  $V(\phi)$ , we shall

introduce the step by *multiplying* the potential by the following function:

$$h_{\text{step}}(\phi) = 1 + \alpha \tanh\left(\frac{\phi - \phi_0}{\Delta\phi}\right), \quad (45)$$

as is often done in the literature [18, 19]. Clearly, the quantities  $\alpha$ ,  $\phi_0$  and  $\Delta\phi$  denote the height, the location and the width of the step, respectively. We shall consider the effects of the introduction of the step in the archetypical quadratic large field model, viz.

$$V(\phi) = \frac{1}{2} m^2 \phi^2, \quad (46)$$

where  $m$  represents the mass of the inflaton, and a small field model governed by the potential

$$V(\phi) = V_0 \left[ 1 - \left(\frac{\phi}{\mu}\right)^p \right]. \quad (47)$$

We shall specifically focus on the case wherein  $p = 4$  and  $\mu = 15 M_{\text{Pl}}$ , as it leads to a tilt that is consistent with the observations, and a smaller tensor-to-scalar ratio (of  $r \simeq 0.01$ ) than the above quadratic potential<sup>§</sup>. The introduction of the step has been shown to lead to a short period of deviation from slow roll inflation, which, in turn, produces a burst of oscillations in the scalar power spectrum, resulting in an improved fit to the data, in both these models [19]. The best fit parameters in the case of the quadratic potential (46) prove to be  $m = 7.147 \times 10^{-6} M_{\text{Pl}}$ ,  $\alpha = 1.606 \times 10^{-3}$ ,  $\phi_0 = 14.67 M_{\text{Pl}}$  and  $\Delta\phi = 0.0311 M_{\text{Pl}}$ . The field is assumed to start on the inflationary attractor at an initial value of  $\phi_i = 16.5 M_{\text{Pl}}$ , so that at least 60 e-folds of inflation takes place. The small field model (47) too is found to lead to a very similar spectrum and an almost identical extent of improvement in the fit to the data. The best fit values of the parameters in this case are found to be  $V_0 = 5.501 \times 10^{-10} M_{\text{Pl}}^4$ ,  $\alpha = -1.569 \times 10^{-4}$ ,  $\phi_0 = 7.888 M_{\text{Pl}}$  and  $\Delta\phi = 9 \times 10^{-3} M_{\text{Pl}}$ . Further, as in the quadratic case, the field is set to start on the attractor. The starting value of the field is chosen to be  $\phi_i = 7.3 M_{\text{Pl}}$ , and it rolls through the step towards  $\phi \simeq \mu$ . Fig. 8 contains an illustration of the potentials corresponding to the quadratic case (46) and the small field model (47) in the presence of the step (45) for the values of the parameters discussed above.

#### 4.2. Oscillations in the inflaton potential

The second class of models that we shall consider are those which lead to small but repeated deviations from slow roll as in the case of models which contain oscillatory terms in the inflaton potential. The first such model that we shall consider is the conventional quadratic potential (46) that is modulated by sinusoidal oscillations as follows [25, 30, 31]:

$$V(\phi) = \frac{1}{2} m^2 \phi^2 \left[ 1 + \alpha \sin\left(\frac{\phi}{\beta} + \delta\right) \right]. \quad (48)$$

<sup>§</sup> It may be worth noting that such rather large values for the parameter  $\mu$  (in Planck units) can be considered to be a drawback of the small field model.



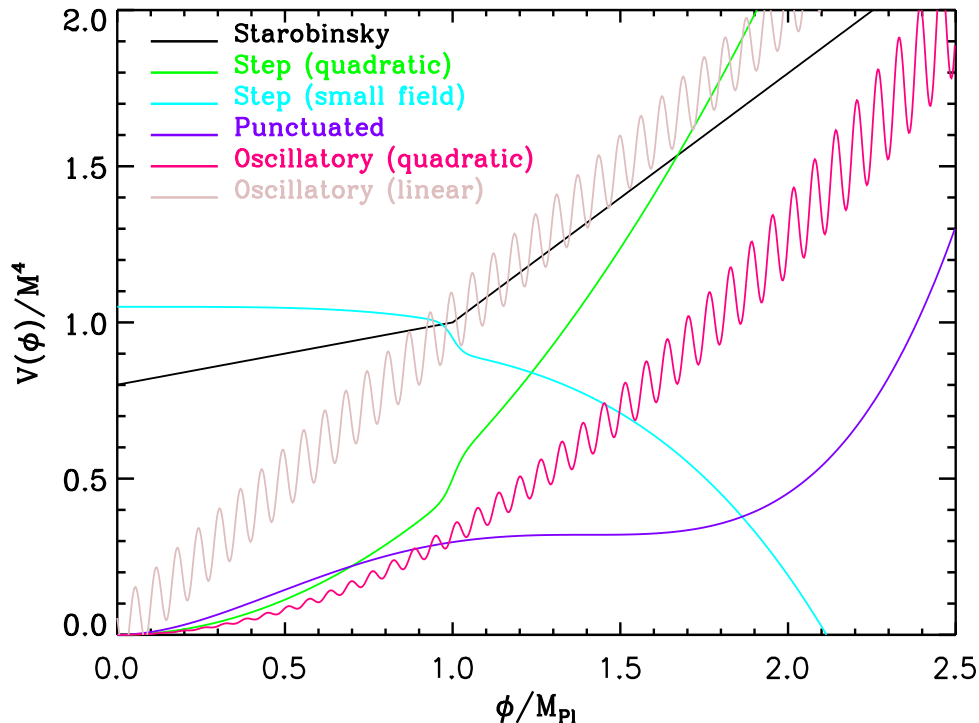


**Figure 8.** An illustration of the potentials in the different models of our interest. The analytical form of the potentials and the values of the parameters are discussed in the text.

The second model that we shall consider in this context is the axion monodromy model which is motivated by string theory [26, 28]. The inflaton potential in such a case is given by

$$V(\phi) = \lambda \left[ \phi + \alpha \cos \left( \frac{\phi}{\beta} + \delta \right) \right]. \quad (49)$$

Evidently, in these potentials, while the parameters  $\alpha$  and  $\beta$  describe the amplitude and the frequency of the superimposed oscillations, the parameter  $\delta$  shifts the oscillations within one period. Note that, whereas the amplitude of the oscillation is fixed in the axion monodromy model, the amplitude depends quadratically on the field in the chaotic model described by the potential (48). The inflaton oscillates as it rolls down these potentials, and these oscillations persist all the way until the end of inflation.

The oscillating inflaton leads to small oscillations in the slow roll parameters (in this context, see, for instance, Ref. [45]), which, as we shall soon illustrate, results in continuing oscillations in the primordial scalar power spectrum. It is found that, in the case of the potential (48), the power spectrum corresponding to  $m = 1.396 \times 10^{-5} M_{\text{Pl}}$ ,  $\alpha = 2.56 \times 10^{-4}$ ,  $\beta = 0.1624 M_{\text{Pl}}$  and  $\delta = 2.256$  leads to a modest improvement in the fit to the CMB data [25, 28]. Whereas, the axion monodromy model (49) leads to a considerable improvement in the fit for the following values of the parameters  $\lambda = 2.513 \times 10^{-10} M_{\text{Pl}}^3$ ,  $\alpha = 1.84 \times 10^{-4} M_{\text{Pl}}$ ,  $\beta = 4.50 \times 10^{-4} M_{\text{Pl}}$  and  $\delta = 0.336$ . While

the field is assumed to start on the inflationary attractor at the initial value of about  $\phi_i = 12 M_{\text{Pl}}$  in the monodromy model, the field is evolved from  $\phi_i = 16 M_{\text{Pl}}$  in the case of the quadratic potential with sinusoidal oscillations [26, 28]. We have plotted the two potentials (48) and (49) in Fig. 8 for the above values of the parameters.

#### 4.3. Punctuated inflaton and the Starobinsky model

We shall consider two models under the last class, both of which are known to lead to brief but sharp departures from slow roll. The first of the inflationary models that we shall consider in this class is described by the following potential containing two parameters  $m$  and  $\lambda$ :

$$V(\phi) = \frac{m^2}{2} \phi^2 - \frac{\sqrt{2\lambda(n-1)}m}{n} \phi^n + \frac{\lambda}{4} \phi^{2(n-1)}. \quad (50)$$

The third quantity  $n$  that appears in the potential is an integer which takes values greater than two. Such potentials are known to arise in certain minimal supersymmetric extensions of the standard model [46]. It is worthwhile noting here that the case of  $n = 3$  has been considered much earlier for reasons similar to what we shall consider here, viz. towards producing certain features in the scalar power spectrum [47]. In the above potential, the coefficient of the  $\phi^n$  term is chosen such that the potential contains a point of inflection at, say,  $\phi = \phi_0$  (i.e. the location where both  $dV/d\phi$  and  $d^2V/d\phi^2$  vanish), so that  $\phi_0$  given by

$$\phi_0 = \left[ \frac{2m^2}{(n-1)\lambda} \right]^{\frac{1}{2(n-2)}}. \quad (51)$$

If one starts at a suitable value of the field beyond the point the inflection in the above potential, it is found that one can achieve two epochs of slow roll inflation sandwiching a brief period of departure from inflation (lasting for a little less than a  $e$ -fold), a scenario which has been dubbed as punctuated inflation [17]. In fact, it is the point of inflection, around which the potential exhibits a plateau with an extremely small curvature, which permits such an evolution to be possible. It is found that the following values for the potential parameters results in a power spectrum that leads to an improved fit to the CMB data in the  $n = 3$  case:  $m = 1.5012 \times 10^{-7} M_{\text{Pl}}$  and  $\phi_0 = 1.95964 M_{\text{Pl}}$ . Fig. 8 contains a plot of the potential (50) corresponding to these values of the parameters. It should be added that the field is assumed to start from rest at an initial value of  $\phi_i = 11.5 M_{\text{Pl}}$  on the potential to arrive at the required behavior.

The second model that we shall consider in the last class is the Starobinsky model [33], which we had briefly discussed in the previous section. As we shall soon illustrate, the model leads to a scalar power spectrum that has a certain resemblance to the spectrum generated by punctuated inflation. The model consists of a linear potential with a sharp change in its slope at a given point, and can be described as follows:

$$V(\phi) = \begin{cases} V_0 + A_+ (\phi - \phi_0) & \text{for } \phi > \phi_0, \\ V_0 + A_- (\phi - \phi_0) & \text{for } \phi < \phi_0. \end{cases} \quad (52)$$

We have illustrated this potential in Fig. 8. Evidently, while the value of the scalar field where the slope changes abruptly is  $\phi_0$ , the slope of the potential above and below  $\phi_0$  are given by  $A_+$  and  $A_-$ , respectively. Moreover, the quantity  $V_0$  denotes the value of the potential at  $\phi = \phi_0$ . A crucial assumption of the Starobinsky model is that the value of  $V_0$  is sufficiently large so that the behavior of the scale factor always remains close to that of de Sitter. The change in the slope causes a short period of deviation from slow roll as the field crosses  $\phi_0$ . However, in contrast to the case of the punctuated inflationary scenario, where one encounters a brief departure from inflation, inflation continues uninterrupted in the Starobinsky model. We have not compared the Starobinsky model with the data, and we shall work with two different sets of values for the parameters of the model. One set corresponds to values of the parameters that allow for the comparison of the analytical results for the bi-spectrum that have been obtained in this case [34, 35] with the corresponding numerical ones. The other set shall be chosen to lead to a spectrum that closely mimics the power spectrum encountered in punctuated inflation. In the case of the former, as we had already mentioned in the caption of Fig. 7, we shall choose the following values of the parameters:  $V_0 = 2.36 \times 10^{-12} M_{\text{Pl}}^4$ ,  $A_+ = 3.35 \times 10^{-14} M_{\text{Pl}}^3$ ,  $A_- = 7.26 \times 10^{-15} M_{\text{Pl}}^3$  and  $\phi_0 = 0.707 M_{\text{Pl}}$ , while, in the case of the latter, we shall work with the same values of  $A_+$  and  $\phi_0$ , but shall set  $V_0 = 2.94 \times 10^{-13} M_{\text{Pl}}^4$ , and  $A_- = 3.35 \times 10^{-16} M_{\text{Pl}}^3$ . Also, we shall work with an initial value of  $\phi_i = 0.849 M_{\text{Pl}}$  in the first instance and with  $\phi_i = 1.8 M_{\text{Pl}}$  in the second. Further, we shall start with field velocities that are determined by the slow roll conditions in both the cases.

#### 4.4. The power spectra

We shall now discuss the scalar power spectra generated by the different inflationary models that we have listed above. We shall highlight here certain aspects of the power spectra that arise in the different class of models.

In Fig. 9, we have illustrated the scalar power spectrum that arises in the different models that we consider. As we had discussed in Sub-sec. 3.3, the standard Bunch-Davies initial conditions are imposed on the perturbations when the modes are well inside the Hubble radius. The modes are evolved on to super Hubble scales, and the spectrum is evaluated when the amplitude of the curvature perturbation has frozen when they are sufficiently outside the Hubble radius. Let us first focus on the power spectra that arise in the Starobinsky model [33] and the punctuated inflationary scenario [17]. Note that, both these models lead to a step like feature as well as a spike in the power spectrum. The spikes arise due to the sharp departure from slow roll that occurs in these models. While the first slow roll parameter  $\epsilon_1$  remains small in the Starobinsky model as the field crosses the transition, the second slow parameter  $\epsilon_2$  turns very large briefly [34, 35]. In the case of punctuated inflation,  $\epsilon_1$  itself grows to a large value thereby actually interrupting inflation for about a e-fold. It is this property that results in a sharper spike in the power spectrum in the case of punctuated inflation than the

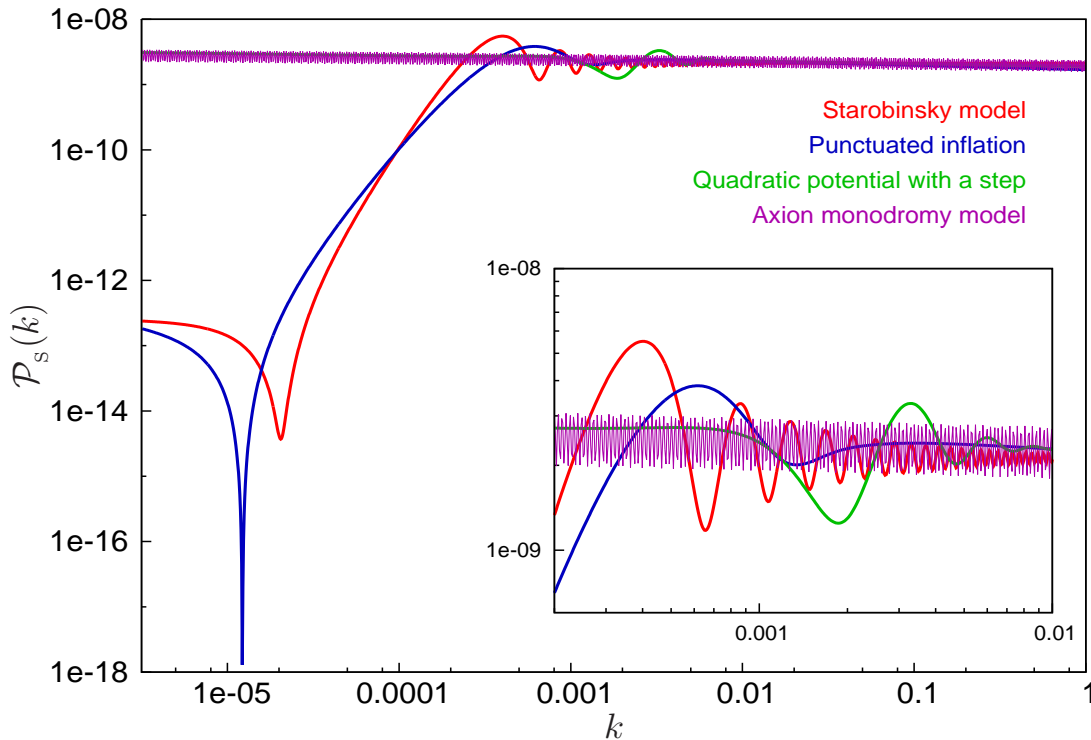


**Figure 9.** The scalar power spectrum in the different types of inflationary models that we consider. The parameters of the Starobinsky model [33] have been chosen such that the resulting power spectrum closely resembles the spectrum that arises in the punctuated inflationary scenario which is known to lead to an improved fit to the CMB data [17]. While the models with a step [18, 19] lead to a burst of oscillations over a specific range of scales, inflaton potentials with oscillating terms produce modulations over a wide range of scales in the power spectrum [26, 28]. The inset highlights the differences in the various power spectra over a smaller range of scales. We have emphasized the important aspects of these different power spectra in some detail in the text.

Starobinsky model. The overall step in these models is easier to understand, and it simply arises due to the difference in the Hubble scales associated with the slow roll epochs before and after the period of fast roll. Both these models also lead to oscillations before the spectra turn nearly scale invariant on small scales. The spectra that arises in punctuated inflation, in addition to leading to a better fit to the outliers at very small multipoles (because of the drop in power on these scales), also provides an improvement in the fit to the outlier at  $\ell \simeq 22$  [17].

Let us now turn to the cases of the models with a step in the potential and the potentials which contain oscillatory terms. In contrast to the Starobinsky model and the punctuated inflationary scenario, these models lead to much milder deviations from slow roll. As a result, they also lead to smaller deviations from a nearly scale invariant power spectrum. In the context of models with a step in the potential, a step at the correct location and of a suitable amplitude leads to a burst of oscillations in the power spectrum

which in turn provides an improved fit to the outliers at  $\ell \simeq 22$  and 40 [18, 19]. It is interesting to note in Fig. 9 that the spectra from punctuated inflation and the model with a step in the potential match briefly as they oscillate near scales corresponding to  $\ell \simeq 22$ . Clearly, it is this behavior that leads to a better fit to the outlier in the data at these scales. While all the models that we have discussed on until now result in localized features, the models with oscillating inflation potentials are somewhat special as they contain non-local features, i.e. they lead to continuing oscillations that extend over a wide range of scales in the power spectrum. Needless to add, they arise due to the persisting oscillations of the scalar field as it rolls up and down the modulations in the potential. Interestingly, these features provide an improved fit to the data over a large range of all scales [26, 28].

## 5. Results in the equilateral limit

We shall now discuss the bi-spectra and the non-Gaussianity parameter  $f_{\text{NL}}$  arrived at numerically in the various models of our interest.

In Fig. 10, we have plotted the various contributions, viz.  $G_1 + G_3$ ,  $G_2$ ,  $G_4 + G_7$  and  $G_5 + G_6$  (in the equilateral limit) for the punctuated inflationary scenario driven by the potential (50), the quadratic potential (46) with the step (45), and the axion monodromy model (49) which contains oscillations in the inflaton potential. These plots (and also the ones in Fig. 7) clearly point to the fact that it is the combination  $G_4 + G_7$  that contributes the most to the scalar bi-spectrum in these cases [30, 31].

In Fig. 11, we have plotted the quantity  $f_{\text{NL}}^{\text{eq}}$  due to the dominant contribution that arises in the various models that we have considered. It is clear from this figure that, while in certain cases  $f_{\text{NL}}^{\text{eq}}$  can prove to be a good discriminator, it cannot help in others, and its ability to discriminate depends strongly on the differences in the background dynamics. For instance, the evolution of the first two slow roll parameters are very similar when a step is introduced in either the quadratic potential or a small field model [19]. Hence, it is not surprising that the  $f_{\text{NL}}^{\text{eq}}$  behaves in a similar fashion in both these models. Whereas,  $f_{\text{NL}}^{\text{eq}}$  proves to be substantially different in punctuated inflation and the Starobinsky model. Recall that, in the Starobinsky model, the first slow roll parameter remains small throughout the evolution. In contrast, it grows above unity for a very short period (leading to a brief interruption of the accelerated expansion) in the punctuated inflationary scenario. It is this departure from inflation that leads to a sharp drop in the power spectrum and a correspondingly sharp rise in the parameter  $f_{\text{NL}}^{\text{eq}}$  in punctuated inflation. In fact, this occurs for modes that leave the Hubble radius just before inflation is interrupted [48]. However, note that,  $f_{\text{NL}}^{\text{eq}}$  grows with  $k$  at large wavenumbers in the Starobinsky model. This can be attributed to the fact that  $\epsilon_2'$ , which determines the contribution due to the fourth term, diverges due to the discontinuity in the second derivative of the potential [35]. But, we should hasten to clarify that this can be shown to be an unphysical artifact arising due to the presence of a Heaviside function in the description of the potential. Similarly, we find that  $f_{\text{NL}}^{\text{eq}}$  is rather large in

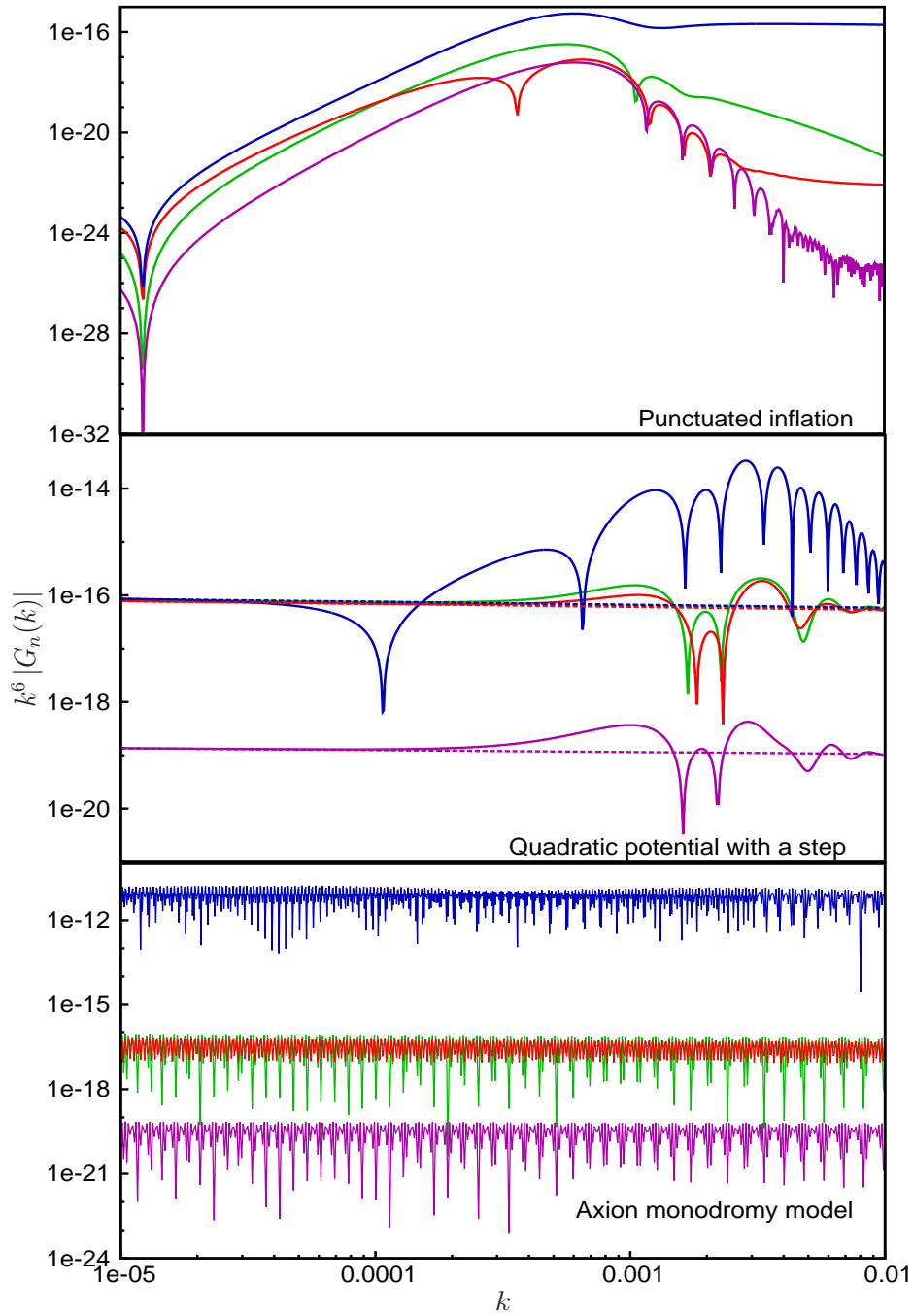


**Figure 10.** The set of quantities  $k^6 |G_n(k)|$  plotted as in Fig. 7 with the same choice of colors to represent the different  $G_n(k)$ . The figures on top, in the middle and at the bottom correspond to punctuated inflation, the quadratic potential with a step and the axion monodromy model, respectively, and they have been plotted for values of the parameters that lead to the best fit to the WMAP data as discussed in the text [17, 19, 28]. In the middle figure, the dashed lines correspond to the quadratic potential when the step is not present.

the axion monodromy model in contrast to the case wherein the conventional quadratic

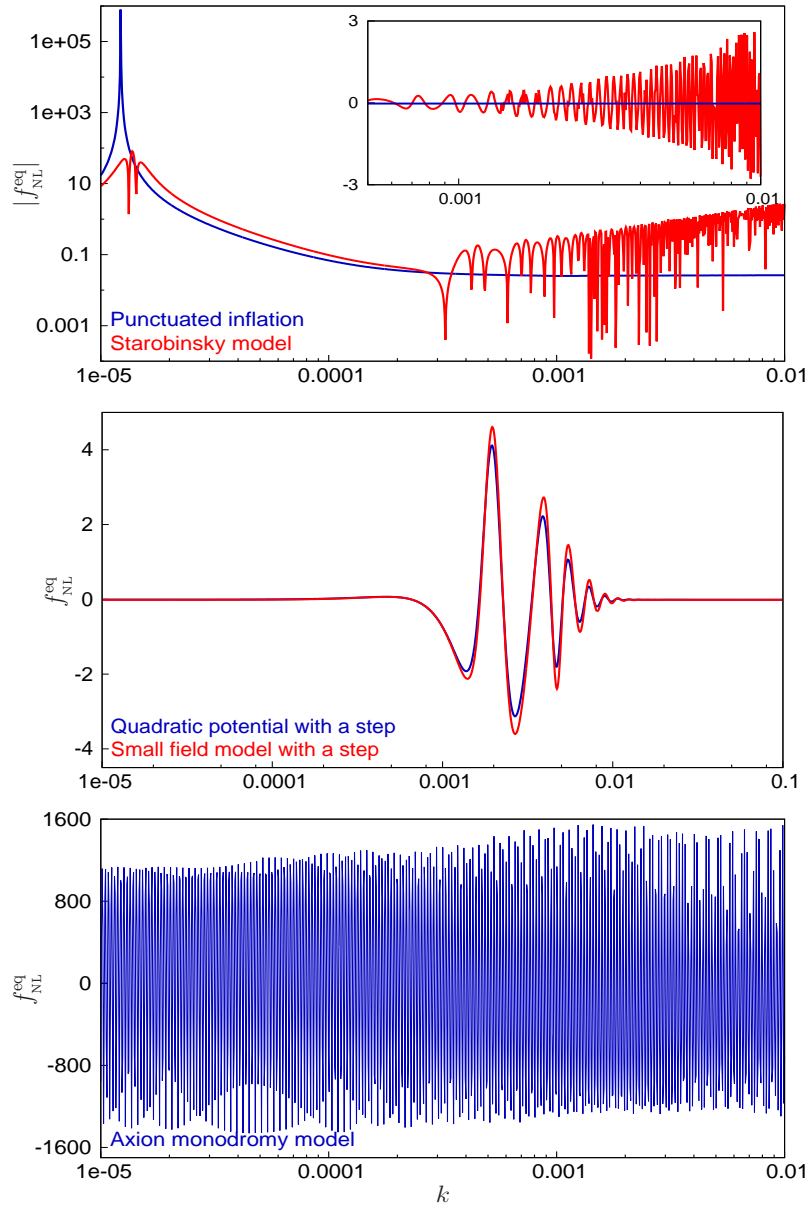


**Figure 11.** A plot of  $f_{NL}^{eq}$  corresponding to the various models that we have considered. The figure at the top contains the absolute value of  $f_{NL}^{eq}$ , plotted on a logarithmic scale (for convenience in illustrating the extremely large values that arise), in the Starobinsky model and the punctuated inflationary scenario. The inset highlights the growth in  $f_{NL}^{eq}$  at large wavenumbers in the case of the Starobinsky model, in conformity with the conclusions that have also been arrived at analytically [35]. The figure in the middle contains  $f_{NL}^{eq}$  for the cases wherein a step has been introduced in a quadratic potential and a small field model. The figure at the bottom corresponds to that of the axion monodromy model. As we have described, these sets of models lead to scalar power spectra with certain common characteristics. Needless to say, while  $f_{NL}^{eq}$  is considerably different in the first and the last sets of models, it is almost the same in the case of models with a step. These similarities and differences can be attributed completely to the background dynamics.

potential is modulated by an oscillatory term. The large value of  $f_{\text{NL}}^{\text{eq}}$  that arises in the monodromy model can be attributed to the resonant behavior encountered in the model [26, 30, 31, 28]. In fact, we have also evaluated the  $f_{\text{NL}}^{\text{eq}}$  for the case of quadratic potential modulated by sinusoidal oscillations, which too leads to continuing, periodic features in the scalar power spectrum [25, 28]. However, we find that the  $f_{\text{NL}}^{\text{eq}}$  in such a case proves to be rather small (of the order  $10^{-2}$  or so).

## 6. Discussion

In this work, we have presented BINGO, a code for the efficient computation of the bi-spectrum and the non-Gaussianity parameter  $f_{\text{NL}}$  in single field inflationary models involving the canonical scalar field. While there has been previous efforts in the literature towards numerically calculating the bi-spectrum and the non-Gaussianity parameter  $f_{\text{NL}}$ , our effort in arriving at BINGO can be said to be more complete for the following four reasons. First and foremost, we have explicitly illustrated that the procedures that BINGO adopts to evaluate the integrals involved are robust. On the one hand, we have converged on a suitable form for the cut off required in the sub-Hubble domain (in particular, the value of the cut off parameter  $\kappa$ ) and the corresponding lower limit of the integrals, after a careful investigation of their effects on the amplitude of the bi-spectrum. On the other, we have shown that the super-Hubble contributions to the complete bi-spectrum are negligible, which allows us to arrive at a convenient upper limit for the integrals. Secondly, BINGO can calculate all the contributions to the bi-spectrum. Thirdly, it can evaluate the bi-spectrum for an arbitrary triangular configuration of the wavevectors. Lastly, we have compared the numerical results from BINGO with the analytical expressions available in certain specific cases, an exercise which illustrates that BINGO can be accurate to better than 5%. As we had mentioned in the introductory section, we have made a version of BINGO, one that focuses on the equilateral limit, available online at <https://www.physics.iitm.ac.in/~sriram/bingo/bingo.html>. Moreover, if needed, as we have pointed out earlier, the level of accuracy of BINGO can be improved by carrying out the integrals from a larger initial value of  $k/(aH)$  (i.e. from an earlier point in time) and simultaneously working with a smaller value of the cut off parameter  $\kappa$ . In fact, in the code that is publicly available, these parameters have been allowed to be set by the user, as is desired.

After presenting BINGO and illustrating the extent of its accuracy, we had made use of the code to examine the power of the non-Gaussianity parameter  $f_{\text{NL}}$  to lift degeneracies between various single field inflationary models involving the canonical scalar field at the level of the power spectrum. With this goal in mind, using BINGO, we have evaluated the quantity  $f_{\text{NL}}^{\text{eq}}$  in a slew of models that generate features in the scalar perturbation spectrum. We find that the amplitude of  $f_{\text{NL}}^{\text{eq}}$  proves to be rather different when the dynamics of the background turns out reasonably different, which, in retrospect, need not be surprising at all. For instance, models such as the punctuated inflationary scenario and the Starobinsky model which lead to very sharp features in



the power spectrum also lead to substantially large  $f_{\text{NL}}$ . Such possibilities can aid us discriminate between the models to some extent. We had focused on evaluating the quantity  $f_{\text{NL}}$  in the equilateral limit. It will be worthwhile to compute the corresponding values in the other limits as well as for the other forms (such as the squeezed and the orthogonal ones) of the non-Gaussianity parameter [7]. In particular, it will be interesting to examine if the so-called consistency relation between the local non-Gaussianity parameter  $f_{\text{NL}}$  and the scalar spectral index in the squeezed limit is valid even in situations wherein extreme deviations from slow roll occur (in this context, see Refs. [30, 31, 42, 49, 50, 51]). Actually, since many of the models leading to features have interesting bi-spectral shapes, it is important that we arrive at the spectral shapes for the various models for an arbitrary triangular configurations of the wavenumbers. It is also important that, apart from computing the local non-Gaussianity parameter as we have done here, one evaluates the corresponding equilateral and the orthogonal parameters as well. We are currently working on extending the scope of BINGO to these cases.

We would like to conclude by highlighting one important point. Having computed the primordial bi-spectrum, the next logical step would be to compute the corresponding CMB bi-spectrum, an issue which we have not touched upon as it is beyond the scope of the current work. While tools seem to be available to evaluate the CMB bi-spectrum based on the first order brightness function, the contribution due to the brightness function at the second order remains to be understood satisfactorily (in this context, see Ref. [52] and the last reference in Ref. [9]). This seems to be an important aspect that is worth investigating closer.

## Acknowledgments

We would like to acknowledge the use of the high performance computing facilities at the Harish-Chandra Research Institute, Allahabad, India (<http://cluster.hri.res.in>). DKH also wishes to acknowledge support from the Korea Ministry of Education, Science and Technology, Gyeongsangbuk-Do and Pohang City for Independent Junior Research Groups at the Asia Pacific Center for Theoretical Physics.

## References

- [1] J. Maldacena, JHEP **0305**, 013 (2003).
- [2] D. Seery and J. E. Lidsey, JCAP **0506**, 003 (2005); X. Chen, Phys. Rev. D **72**, 123518 (2005); X. Chen, M.-x. Huang, S. Kachru and G. Shiu, JCAP **0701**, 002 (2007); D. Langlois, S. Renaux-Petel, D. A. Steer and T. Tanaka, Phys. Rev. Lett. **101**, 061301 (2008); Phys. Rev. D **78**, 063523 (2008).
- [3] X. Chen, Adv. Astron. **2010**, 638979 (2010).
- [4] A. Gangui, F. Lucchin, S. Matarrese and S. Mollerach, Astrophys. J. **430**, 447 (1994); A. Gangui, Phys. Rev. D **50**, 3684 (1994); A. Gangui and J. Martin, Mon. Not. Roy. Astron. Soc. **313**, 323 (2000); L. Wang and M. Kamionkowski, Phys. Rev. D **61**, 063504 (2010).

- [5] J. Dunkley *et al.*, *Astrophys. J. Suppl.* **180**, 306 (2009); E. Komatsu *et al.*, *Astrophys. J. Suppl.* **180**, 330 (2009).
- [6] D. Larson *et al.*, *Astrophys. J. Suppl.* **192**, 16 (2011); E. Komatsu *et al.*, *Astrophys. J. Suppl.* **192**, 18 (2011).
- [7] C. L. Bennett *et al.*, arXiv:1212.5225v1 [astro-ph.CO]; G. Hinshaw *et al.*, arXiv:1212.5226v1 [astro-ph.CO].
- [8] E. Komatsu and D. N. Spergel, *Phys. Rev. D* **63**, 063002 (2001); E. Komatsu, D. N. Spergel and B. D. Wandelt, *Astrophys. J.* **634**, 14 (2005); D. Babich and M. Zaldarriaga, *Phys. Rev. D* **70**, 083005 (2004); M. Liguori, F. K. Hansen, E. Komatsu, S. Matarrese and A. Riotto, *Phys. Rev. D* **73**, 043505 (2006); C. Hikage, E. Komatsu and T. Matsubara, *Astrophys. J.* **653** (2006) 11 (2006); J. R. Fergusson and E. P. S. Shellard, *Phys. Rev. D* **76**, 083523 (2007); A. P. S. Yadav, E. Komatsu and B. D. Wandelt, *Astrophys. J.* **664**, 680 (2007); P. Creminelli, L. Senatore and M. Zaldarriaga, *JCAP* **0703**, 019 (2007); A. P. S. Yadav and B. D. Wandelt, *Phys. Rev. Lett.* **100**, 181301 (2008); C. Hikage, T. Matsubara, P. Coles, M. Liguori, F. K. Hansen and S. Matarrese, *Mon. Not. Roy. Astron. Soc.* **389**, 1439 (2008); O. Rudjord, F. K. Hansen, X. Lan, M. Liguori, D. Marinucci and S. Matarrese, *Astrophys. J.* **701**, 369 (2009); K. M. Smith, L. Senatore and M. Zaldarriaga, *JCAP* **0909**, 006 (2009); J. Smidt, A. Amblard, C. T. Byrnes, A. Cooray, A. Heavens and D. Munshi, *Phys. Rev. D* **81**, 123007 (2010); J. R. Fergusson, M. Liguori and E. P. S. Shellard, arXiv:1006.1642v2 [astro-ph.CO].
- [9] M. Liguori, E. Sefusatti, J. R. Fergusson and E. P. S. Shellard, *Adv. Astron.* **2010**, 980523 (2010); A. P. S. Yadav and B. D. Wandelt, arXiv:1006.0275v3 [astro-ph.CO]; E. Komatsu, *Class. Quantum Grav.* **27**, 124010 (2010).
- [10] H. Funakoshi and S. Renaux-Petel, arXiv:1211.3086v1 [astro-ph.CO].
- [11] E. W. Kolb and M. S. Turner, *The Early Universe* (Addison-Wesley, Redwood City, California, 1990); S. Dodelson, *Modern Cosmology* (Academic Press, San Diego, U.S.A., 2003); V. F. Mukhanov, *Physical Foundations of Cosmology* (Cambridge University Press, Cambridge, England, 2005); S. Weinberg, *Cosmology* (Oxford University Press, Oxford, England, 2008); R. Durrer, *The Cosmic Microwave Background* (Cambridge University Press, Cambridge, England, 2008); D. H. Lyth and A. R. Liddle, *The Primordial Density Perturbation* (Cambridge University Press, Cambridge, England, 2009); P. Peter and J-P. Uzan, *Primordial Cosmology* (Oxford University Press, Oxford, England, 2009); H. Mo, F. v. d. Bosch and S. White, *Galaxy Formation and Evolution* (Cambridge University Press, Cambridge, England, 2010).
- [12] H. Kodama and M. Sasaki, *Prog. Theor. Phys. Suppl.* **78**, 1 (1984); V. F. Mukhanov, H. A. Feldman and R. H. Brandenberger, *Phys. Rep.* **215**, 203 (1992); J. E. Lidsey, A. Liddle, E. W. Kolb, E. J. Copeland, T. Barreiro and M. Abney, *Rev. Mod. Phys.* **69**, 373 (1997); D. H. Lyth and A. Riotto, *Phys. Rep.* **314**, 1 (1999); A. Riotto, arXiv:hep-ph/0210162; J. Martin, *Braz. J. Phys.* **34**, 1307 (2004); *Lect. Notes Phys.* **669**, 199 (2005); *Lect. Notes Phys.* **738**, 193 (2008); B. Bassett, S. Tsujikawa and D. Wands, *Rev. Mod. Phys.* **78**, 537 (2006); W. H. Kinney, arXiv:0902.1529 [astro-ph.CO]; L. Sriramkumar, *Curr. Sci.* **97**, 868 (2009); D. Baumann, arXiv:0907.5424v1 [hep-th].
- [13] J. Martin, C. Ringeval and R. Trotta, *Phys. Rev. D* **83**, 063514 (2011).
- [14] H. V. Peiris *et al.*, *Astrophys. J. Suppl.* **148**, 213 (2003).
- [15] S. Hannestad, *Phys. Rev. D* **63**, 043009 (2001); S. L. Bridle, A. M. Lewis, J. Weller and G. Efstathiou, *Mon. Not. Roy. Astron. Soc.* **342**, L72 (2003); P. Mukherjee and Y. Wang, *Astrophys. J.* **599**, 1 (2003); S. Hannestad, *JCAP* **0404**, 002 (2004); A. Shafieloo and T. Souradeep, *Phys. Rev. D* **70**, 043523 (2004); D. Tocchini-Valentini, Y. Hoffman and J. Silk, *Mon. Not. Roy. Astron. Soc.* **367**, 1095 (2006); A. Shafieloo, T. Souradeep, P. Manimaran, P. K. Panigrahi and R. Rangarajan, *Phys. Rev. D* **75**, 123502 (2007); A. Shafieloo and T. Souradeep, *Phys. Rev. D* **78**, 023511 (2008); R. Nagata and J. Yokoyama, *Phys. Rev. D* **79**, 043010 (2009); G. Nicholson and C. R. Contaldi, *JCAP* **0907**, 011 (2009).
- [16] B. Feng and X. Zhang, *Phys. Lett. B* **570**, 145 (2003); M. Kawasaki and F. Takahashi, *Phys. Lett.*

- B **570**, 151 (2003); R. Sinha and T. Souradeep, Phys. Rev. D **74**, 043518 (2006); M. J. Mortonson and W. Hu, Phys. Rev. D **80**, 027301 (2009).
- [17] R. K. Jain, P. Chingangbam, J.-O. Gong, L. Sriramkumar and T. Souradeep, JCAP **0901**, 009 (2009); R. K. Jain, P. Chingangbam, L. Sriramkumar and T. Souradeep, Phys. Rev. D **82**, 023509 (2010).
- [18] J. A. Adams, B. Cresswell and R. Easther, Phys. Rev. D **64**, 123514 (2001); L. Covi, J. Hamann, A. Melchiorri, A. Slosar and I. Sorbera, Phys. Rev. D **74**, 083509 (2006); J. Hamann, L. Covi, A. Melchiorri and A. Slosar, Phys. Rev. D **76**, 023503 (2007); M. J. Mortonson, C. Dvorkin, H. V. Peiris and W. Hu, Phys. Rev. D **79**, 103519 (2009).
- [19] D. K. Hazra, M. Aich, R. K. Jain, L. Sriramkumar and T. Souradeep, JCAP **1010**, 008 (2010).
- [20] M. Benetti, M. Lattanzi, E. Calabrese and A. Melchiorri, Phys. Rev. D **84**, 063509 (2011).
- [21] M. Joy, V. Sahni, A. A. Starobinsky, Phys. Rev. D **77**, 023514 (2008); M. Joy, A. Shafieloo, V. Sahni, A. A. Starobinsky, JCAP **0906**, 028 (2009).
- [22] P. Hunt and S. Sarkar, Phys. Rev. D **70**, 103518 (2004); Phys. Rev. D **76**, 123504 (2007); M. Kawasaki, F. Takahashi and T. Takahashi, Phys. Letts. B **605**, 223 (2005); J.-O. Gong, JCAP **0507**, 015 (2005); A. Ashoorioon and A. Krause, arXiv:hep-th/0607001v1; A. Ashoorioon, A. Krause and K. Turzyski, JCAP **0902**, 014 (2009); M. Kawasaki and K. Miyamoto, arXiv:1010.3095v2 [astro-ph.CO]; A. Achucarro, J.-O. Gong, S. Hardeman, G. A. Palma and S. P. Patil, JCAP **1101**, 030 (2011); K. Kumazaki, S. Yokoyama and N. Sugiyama, JCAP **1112**, 008 (2011).
- [23] J. M. Cline, P. Crotty and J. Lesgourgues, JCAP **0309**, 010 (2003); C. R. Contaldi, M. Peloso, L. Kofman and A. Linde, JCAP **0307**, 002 (2003); L. Sriramkumar and T. Padmanabhan, Phys. Rev. D **71**, 103512 (2005); D. Boyanovsky, H. J. de Vega and N. G. Sanchez, Phys. Rev. D **74**, 123006 (2006); Phys. Rev. D **74**, 123007 (2006); B. A. Powell and W. H. Kinney, Phys. Rev. D **76**, 063512 (2007); C. Destri, H. J. de Vega and N. G. Sanchez, Phys. Rev. D **78**, 023013 (2008).
- [24] J. Martin and C. Ringeval, Phys. Rev. D **69**, 083515 (2004); Phys. Rev. D **69**, 127303 (2004); JCAP **0501**, 007 (2005); M. Zarei, Phys. Rev. D **78**, 123502 (2008).
- [25] C. Pahud, M. Kamionkowski and A. R. Liddle, Phys. Rev. D **79**, 083503 (2009).
- [26] R. Flauger, L. McAllister, E. Pajer, A. Westphal and G. Xu, JCAP **1006**, 009 (2010); R. Flauger and E. Pajer, JCAP **1101**, 017 (2011).
- [27] T. Kobayashi and F. Takahashi, JCAP **1101**, 026 (2011).
- [28] M. Aich, D. K. Hazra, L. Sriramkumar and T. Souradeep, arXiv:1106.2798v2 [astro-ph.CO]
- [29] M. Bridges, F. Feroz, M. P. Hobson and A. N. Lasenby, Mon. Not. Roy. Astron. Soc. **400**, 1075 (2009); H. V. Peiris and L. Verde, Phys. Rev. D **81**, 021302 (2010); Z.-K. Guo, D. J. Schwarz and Y.-Z. Zhang, JCAP **1108**, 031 (2011).
- [30] X. Chen, R. Easther and E. A. Lim, JCAP **0706**, 023 (2007); JCAP **0804**, 010 (2008).
- [31] S. Hotchkiss and S. Sarkar, JCAP **1005**, 024 (2010); S. Hannestad, T. Haugbolle, P. R. Jarnhus and M. S. Sloth, JCAP **1006**, 001 (2010); R. Flauger and E. Pajer, JCAP **1101**, 017 (2011); P. Adshead, W. Hu, C. Dvorkin and H. V. Peiris, Phys. Rev. D **84**, 043519 (2011); P. Adshead, C. Dvorkin, W. Hu and E. A. Lim, Phys. Rev. D **85**, 023531 (2012).
- [32] A. Gangui, J. Martin and M. Sakellariadou, Phys. Rev. D **66**, 083502 (2002); R. Holman and A. J. Tolley, JCAP **0805**, 001 (2008); W. Xue and B. Chen, Phys. Rev. D **79**, 043518 (2009); P. D. Meerburg, J. P. van der Schaar and P. S. Corasaniti, JCAP **0905**, 018 (2009); X. Chen, JCAP **1012**, 003 (2010); A. Ashoorioon and G. Shiu, JCAP **1103**, 025 (2011); S. Kundu, JCAP **1202**, 005 (2012); P. D. Meerburg, R. Wijers and J. P. van der Schaar, Mon. Not. Roy. Astron. Soc. **421**, 369 (2012).
- [33] A. A. Starobinsky, Sov. Phys. JETP Lett. **55**, 489 (1992).
- [34] J. Martin and L. Sriramkumar, JCAP **1201**, 008 (2012).
- [35] F. Arroja, A. E. Romano and M. Sasaki, Phys. Rev. D **84**, 123503 (2011); F. Arroja and M. Sasaki, JCAP **1208**, 012 (2012).
- [36] D. K. Hazra, J. Martin and L. Sriramkumar, Phys. Rev. D **86**, 063523 (2012).

- [37] T. Bunch and P. C. W. Davies, Proc. Roy. Soc. Lond. A **360**, 117 (1978).
- [38] D. S. Salopek, J. R. Bond and J. M. Bardeen, Phys. Rev. D **40**, 1753 (1989); C. Ringeval, Lect. Notes Phys. **738**, 243 (2008).
- [39] C. Dvorkin and W. Hu, Phys. Rev. D **81**, 023518 (2010); W. Hu, Phys. Rev. D **84**, 027303 (2011).
- [40] R. W. Brankin, I. Gladwell and L. F. Shampine, *RKSUITE: A suite of Runge-Kutta codes for the initial value problem for ODEs*, Softreport 92-S1, Department of Mathematics, Southern Methodist University, Dallas, Texas, U.S.A, 1992.
- [41] See, for instance, <http://www.netlib.org/> and <http://www.nag.com/>.
- [42] J. Martin, H. Motohashi and T. Suyama, arXiv:1211.0083v1 [astro-ph.CO].
- [43] L. F. Abbott and M. B. Wise, Nucl. Phys. B **244**, 541 (1984); D. H. Lyth and E. D. Stewart, Phys. Lett. B **274**, 168 (1992); J. Martin and D. J. Schwarz, Phys. Rev. D **57**, 3302 (1998).
- [44] See, <http://www.wolfram.com/>.
- [45] D. K. Hazra, arXiv:1210.7170v1 [astro-ph.CO].
- [46] R. Allahverdi, J. Garcia-Bellido, K. Enqvist and A. Mazumdar Phys. Rev. Lett. **97**, 191304 (2006); R. Allahverdi, K. Enqvist, J. Garcia-Bellido, A. Jokinen and A. Mazumdar, JCAP **0706**, 019 (2007); J. C. B. Sanchez, K. Dimopoulos and D. H. Lyth, JCAP **0701**, 015 (2007).
- [47] H. M. Hodges, G. R. Blumenthal, L. A. Kofman and J. R. Primack, Nucl. Phys. B **335**, 197 (1990).
- [48] R. K. Jain, P. Chingangbam and L. Sriramkumar, JCAP **0710**, 003 (2007).
- [49] P. Creminelli and M. Zaldarriaga, JCAP 0410, 006 (2004).
- [50] S. Renaux-Petel, JCAP 1010, 020 (2010).
- [51] X. Chen, H. Firouzjahi, M. H. Namjoo and M. Sasaki, arXiv:1301.5699v1 [hep-th].
- [52] C. Pitrou, J.-P. Uzan and F. Bernardeau, JCAP **1007**, 003 (2010).